LAWRENCE
LIVERMORE
NATIONAL
LABORATORY

UCRL-TR-221283

Contact Interface Verification for DYNA3D

Scenario 1: Basic Contact

Larry D. McMichael

March 31, 2006

This work was performed under the auspices of the U.S. Department of Energy by University of California, Lawrence Livermore National Laboratory under Contract W-7405-Eng-48.

TABLE OF CONTENTS

Contact Interface Verification for DYNA3D
Scenario 1: Basic Contact

Larry D. McMichael
Defense Systems Analysis Group
New Technologies Engineering Division

1 INTRODUCTION

A suite of test problems has been developed to examine contact behavior within the nonlinear, three-dimensional, explicit finite element analysis (FEA) code DYNA3D (Lin, 2005). The test problems address the basic functionality of the contact algorithms, including the behavior of various kinematic, penalty, and Lagrangian enforcement formulations. The results from the DYNA3D analyses are compared to closed form solutions to verify the contact behavior. This work was performed as part of the Verification and Validation efforts of LLNL W Program within the NNSA's Advanced Simulation and Computing (ASC) Program.

DYNA3D models the transient dynamic response of solids and structures including the interactions between disjoint bodies (parts). A wide variety of contact surfaces are available to represent the diverse interactions possible during an analysis, including relative motion (sliding), separation and gap closure (voids), and fixed relative position (tied). The problem geometry may be defined using a combination of element formulations, including one-dimensional beam and truss elements, two-dimensional shell elements, and three-dimensional solid elements. Consequently, it is necessary to consider various element interactions for each contact algorithm being verified.

Most of the contact algorithms currently available in DYNA3D are examined; the exceptions are the Type 4 – Single Surface Contact and Type 11 – SAND algorithms. It is likely that these algorithms will be removed since their functionality is embodied in other, more robust, contact algorithms. The automatic contact algorithm is evaluated using the Type 12 interface. Two other variations of automatic contact, Type 13 and Type 14, offer additional means to adapt the interface domain, but share the same search and restoration algorithms as Type 12. The contact algorithms are summarized in Table 1.

This report and associated test problems examine the scenario where one contact surface exists between two disjoint bodies. These test problems focus on whether a particular contact algorithm properly represents the interactions along the interface. A companion report (McMichael, 2006) and test problems address the multi-contact scenario in which multiple bodies interact with each other via multiple interfaces. The multi-contact test problems examine whether any ordering issues exist in the contact logic.

The test problems are analyzed using version 5.2 (compiled on 12/22/2005) of DYNA3D. The analytical results are used to form baseline solutions for subsequent regression testing.

In section 2, the test problem and contact algorithms are presented. First, the response of a simple, two-block system is developed to establish the expected results for three different contact idealizations. Section 3 discusses the finite element representation of the generic problem. The data extracted from each analysis to satisfy the verification criteria is examined next in section 4, followed by the expected results for each interface idealization in section 5. Section 6 considers the response of each contact algorithm. Finally, section 7 summarizes the observed interface behavior.

Type	Description	Enforcement	Element Formulations
1	Sliding Only	Kinematic	Solid, Shell
2	Tied	Kinematic	Solid, Shell
3	Sliding with voids and friction	Penalty, Lagrange	Solid, Shell
5	Discrete nodes impacting surface	Penalty, Lagrange	Solid, Shell (for master surface)
6	Discrete nodes tied to surface	Kinematic	Solid, Shell (for master surface)
7	Shell edge tied to shell surface	Kinematic	Shell
8	Nodes spotwelded to surface	Penalty	Solid, Shell (for master surface)
9	Tied with failure	Penalty	Solid, Shell
10	One-way algorithm for sliding, Separation, and friction	Penalty, Lagrange	Solid, Shell
12	Automatic contact	Penalty, Lagrange	Solid, Shell

Table 1. Summary of contact algorithms evaluated in this study.

2 BASIC CONTACT PROBLEM

A simple, two-body system is used to isolate the behavior of the individual contact algorithms for different enforcement options, element interactions, and interface options. The generic, single contact interface problem consists of a simple, two-body system as depicted schematically in Figure 1. The forces P_x and P_y are applied with a prescribed magnitude. The lower block is constrained against movement in the y-direction along its bottom surface and against movement in the x-direction along its right side (positive x-face). The dimensions of the upper and lower blocks are 1 unit x 1 unit x 1 unit and 1.51 units x 1 unit x 1.02 units, respectively. The lower block is physically larger to ensure that the upper block remains fully seated during tangential motion in the x-direction.

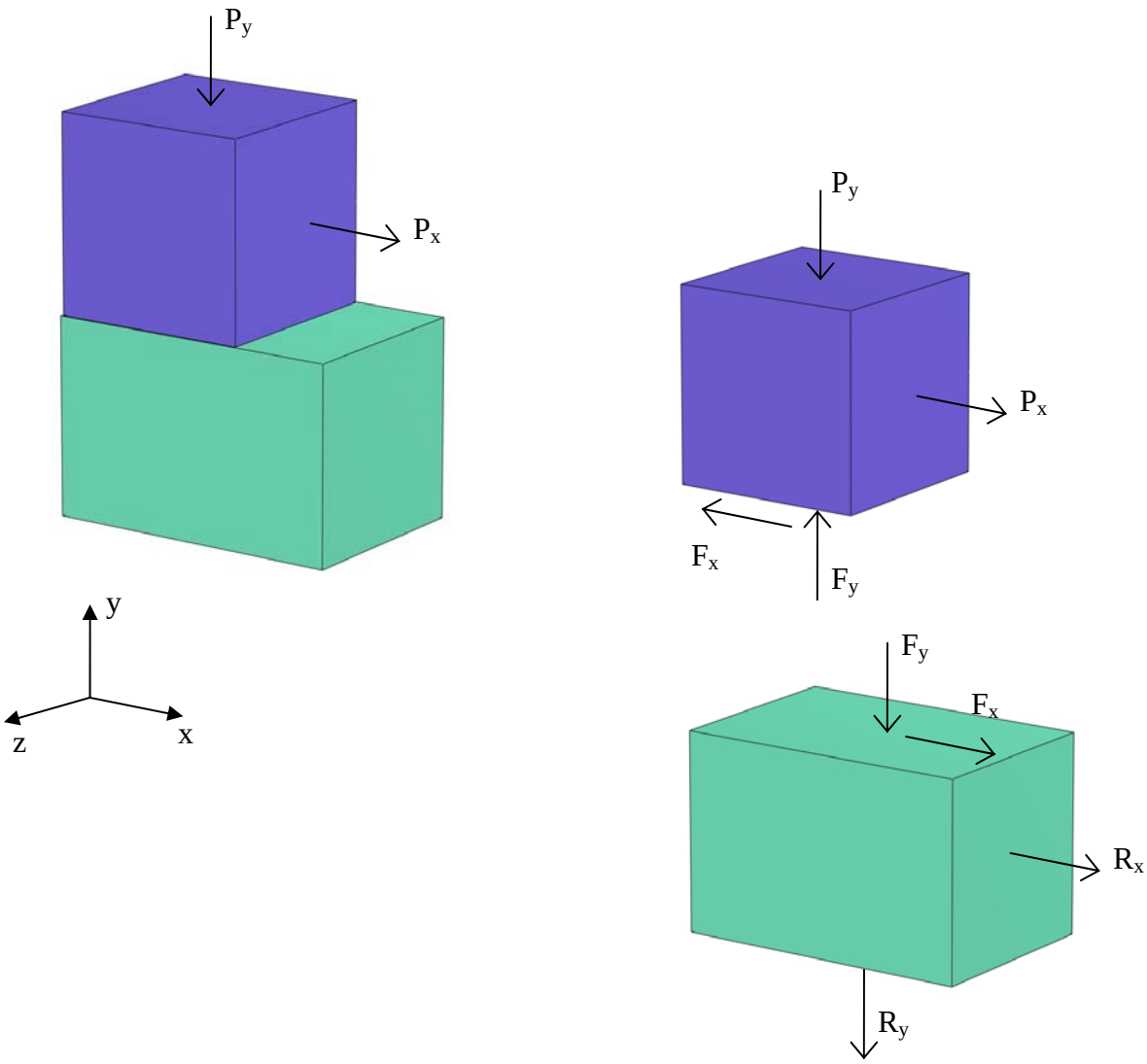

Figure 1. The interface and reaction forces are determined from equilibrium considerations for the basic contact problem.

This simple test problem facilitates the development of closed form solutions under quasi-static conditions. Inertia effects can be ignored when the blocks are stationary or moving with constant velocity. Under these conditions, static equilibrium considerations are used to determine the interface force, F, developed along the x-z plane between the blocks and the reaction force, R, acting against the constraints on the lower block. Since there is no applied load in the z-direction, the interface force and the reaction force in the z-direction are zero. The force components acting perpendicular to the interface (i.e., in the y-direction) are independent of the idealization used for the interface behavior in the tangential (i.e., x) direction. Consequently, the normal forces are determined solely from equilibrium considerations. On the upper block, the interface normal force, F_y, is equal in magnitude to the prescribed force P_y, but acts in the opposite direction. On the lower block, the reaction force in the y-direction, R_y, is equal in magnitude and direction to F_y and, therefore, is also equal to P_y. The tangential interface force component, F_x, resists movement in the plane of the interface and depends upon the interface idealization used.

2.1 INTERFACE IDEALIZATIONS

Three interface idealizations are examined: tied, frictional, and frictionless. A tied interface prevents relative motion between the upper and lower block. The expected interface and reaction forces are determined from equilibrium considerations. On the upper block, the magnitude of F_x is equal to P_x and acts in the opposite direction as the applied force. The magnitude of R_x is also equal to P_x and acts in the same direction as the applied force. The interface would behave in the same manner if the direction of the applied loads was reversed (i.e., a tensile load was applied to the upper block), and there would be a corresponding sign change in the expected interface and reaction forces.

A frictional interface prevents relative normal motion (i.e., no interpenetration of the bodies), but allows relative tangential motion according to a friction model. A traditional Coulomb model is used to idealize the frictional behavior between the two bodies. The maximum static friction force, f_s, is given by the product of the normal force, N, and the coefficient of static friction, μ_s, ($f_s = \mu_s$ N) and the dynamic friction force, f_k, is given by the product of the normal force and the coefficient of kinetic friction, μ_k ($f_k = \mu_k$ N). In the basic contact problem, F_y corresponds to the normal force N = P_y. On the upper block, the interface force F_x acts in the opposite direction of the applied force and is equal to P_x until f_s is exceeded, at which point relative motion is induced and F_x is equal to f_k.

While a frictionless interface prevents relative motion normal to the interface, there is no resistance to relative tangential motion. The interface force F_x and reaction force R_x are therefore equal to zero regardless of the value of P_x.

3 FINITE ELEMENT REPRESENTATION

The assumptions and approximations used in the FEA model to represent the two-body contact problem described in section 2 are discussed. The interface between the upper and lower blocks is idealized as being tied, frictional, or frictionless and is portrayed by a slide surface that enforces the corresponding idealization. The slave surface (or slave nodes) is defined on the upper block, and the master surface is defined on the lower block. The results for each contact algorithm are discussed in section 6. Boundary conditions are specified on the lower block using prescribed displacements. The lower block's displacements are constrained in the x-direction along the right side and in the y-direction along the bottom. Prescribed displacements were selected since DYNA3D outputs the reaction force required to enforce these boundary conditions. The keyword `exact_output_time` is utilized to reduce machine-to-machine variations in the state data for both the printed output file and the Mili plot database. Generalized Rayleigh mass proportional damping is used to suppress the oscillations observed in the transient dynamic response. The fraction of critical damping used is 0.05 (5%) at a frequency of 150 radians/second, where the frequency was determined from the oscillations seen in an undamped analysis. The finite element models of the test problems share several other common aspects, including: the spatial discretization, the representation of friction, the method of applied load, and the material behavior.

3.1 SPATIAL DISCRETIZATION

The spatial domain of each block is represented using shell or solid elements. The discretization in the contact plane determines the interface segments in the case of surface contact and the interface nodes in the case of discrete contact. The upper (slave) block has three elements per unit length in the x-direction and three elements per unit length in the z-direction. The lower (master) block has two elements per unit length in the x-direction and two elements per unit length in the z-direction. As a result of this discretization and the physical dimensions of the blocks, the nodes on the master and slave surfaces are not initially coincident and surface contact problems have a slave-to-master segment ratio of 3:2 per unit length. When solid elements (bricks) are used to represent a body, two elements are used in the y-direction.

The different element interactions possible for a particular contact algorithm are modeled using multiple pairs of upper and lower blocks within a single FE input deck. This approach allows a single test problem to evaluate all of the element combination possible for a given contact algorithm. In the case of surface contact (Types 1, 2, 3, 10, 12), there are three pairs of blocks representing the possible element interactions of solid-on-solid, shell-on-solid, and shell-on-shell contact (refer to Figure 2). In the shell-on-shell problem, a layer of shell elements is bonded to the top surface of the lower block and constitutes the master surface. Boundary conditions are applied to the brick elements to constrain the lower block's movement without overly restricting the deformation of the shell elements and hence the master surface. This results in a better evaluation of shell-on-shell contact since the master and slave surfaces are able to interact and deform. The Type 9 (Tied with failure) interface is valid only for solid (brick) elements, so only solid-on-solid interaction is considered.

The discrete contact algorithms (Types 5, 6, and 8) are single pass formulations that check for contact/penetration of the slave nodes with the master surface. The master surface is formed by

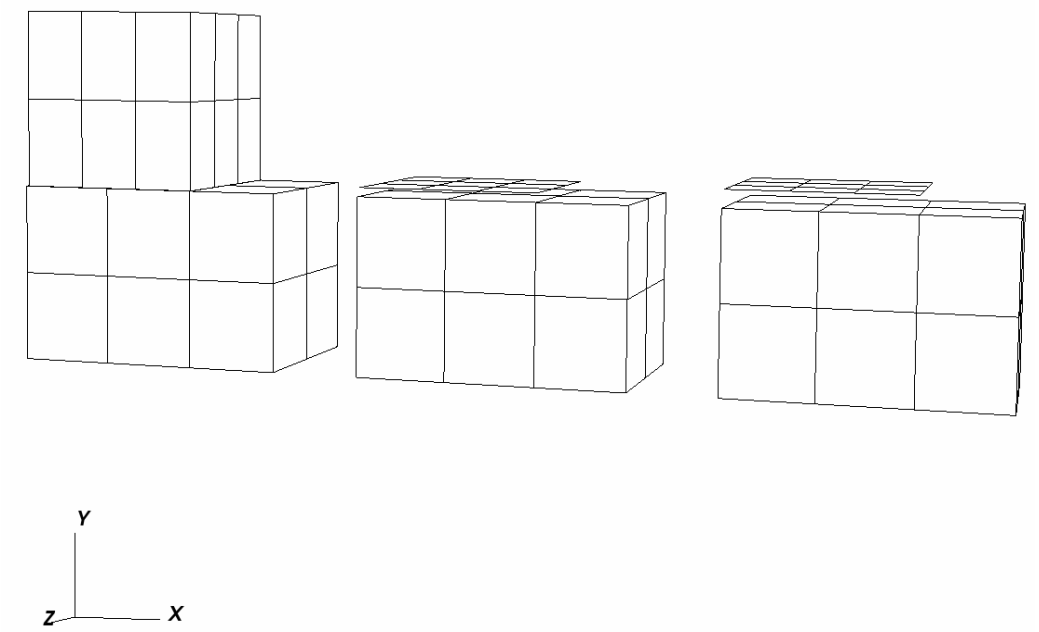

Figure 2. Three types of element interaction are possible for surface contact problems: solid-on-solid, shell-on-solid, and shell-on-shell.

either shell or solid elements, whereas the contact algorithms are independent of the element type associated with the slave nodes. For convenience, shell elements are used to represent the upper block, although beam or truss elements could have been used as well to generate the slave nodes. This representation results in two pairs of blocks corresponding to node-on-solid and node-on-shell interaction. The Type 7 interface is specialized for a shell edge tied to a shell surface. Therefore, a single pair of blocks representing node-on-shell interaction is considered for the Type 7 interface.

Some contact algorithms (Types 3, 5, 10, and 12) account for an offset distance between the master and slave surfaces, either by default or by an interface option. The offset distance for Types 3, 10, and 12 is the shell element thickness. The offset is apparent in Figure 2 as a gap between the upper and lower bodies for the shell-on-solid and shell-on-shell scenarios. When the thickness flag is specified for Type 5 interfaces, only the master surface is offset by half the shell element thickness; however, an optional nodal radius can be assigned to the slave nodes to also account for thickness. In problems that employ Type 5 interfaces, the radius is set to one-half the shell element thickness. Under these conditions, the shell-on-solid gap is one-half the shell element thickness, and the shell-on-shell gap is equal to the shell element thickness.

3.2 COEFFICIENTS OF FRICTION

Frictional behavior in DYNA3D is represented using three coefficients. The coefficient of static friction, μ_s, the coefficient of kinetic friction, μ_k, and an exponential decay coefficient, β. The transition between static and dynamic friction is controlled by β and the relative velocity between the two (master and slave) surfaces. In the test problems, the Lagrange enforcement methods are more sensitive to the value of β. Therefore, a smaller β value is used for the

Lagrange methods than the penalty methods. The friction coefficients used for the verification analyses are given in Table 2. The difference between the static and kinetic friction coefficients is kept relatively small to limit the amount of force accelerating the upper block. This reduces the dynamic effects introduced to the problem and limits the velocity of the upper block, preventing it from sliding off of the lower block during the analysis.

Coefficient of Static Friction, μ_s	0.30
Coefficient of Kinetic Friction, μ_k	0.25
Exponential Decay Coefficient, β (penalty enforcement)	2.0
Exponential Decay Coefficient, β (Lagrange enforcement)	1.3

Table 2. The friction coefficients used for frictional interfaces.

3.3 APPLIED LOADS

The applied force magnitudes are selected to: 1) provide a sufficient normal force to suppress "chatter" along the interface without causing excessive deformation in either the upper or lower blocks, and 2) apply a large enough tangential force to initiate movement without inducing large accelerations in the upper block. In addition to forming the basis for generating frictional forces, the normal force created by P_y acts to maintain contact between the master and slave surfaces as the upper block slides across the lower block. Small variations in the interface force are created by the contact algorithm (e.g., numerical perturbations resulting from a slave node passing from one master segment to another) and inertial effects (e.g., stress wave propagation). If the normal force is too small relative to these variations, then small gaps can open and close over time (i.e., "chatter") and introduce undesired dynamic effects into the solution that obscure the algorithmic behavior. However, the normal force cannot be arbitrarily large since significant curvature develops along the interface if the normal force is too large. The correlation between the interface forces and the applied forces is lost as the interface force decomposition (into normal and tangential components) becomes dependent upon the deformed geometry. If the material stiffness is increased to counteract the greater applied loads, then the computational time and cost to perform the analysis is increased. The increased stiffness results in a smaller time-step size for the dynamic analysis and also requires the loads to be applied more slowly in order to minimize inertial effects.

Balancing these considerations, the selected magnitude for P_y was ten units. Given μ_s and μ_k from Table 2 and that the expected normal force is equal to P_y, then the expected maximum static friction force is f_s = 3.0 and the expected dynamic friction force is f_k = 2.5. For frictional interfaces, the applied body force P_x must be greater than f_s. For frictionless interfaces, P_x can be arbitrarily small since there is no frictional resistance to overcome. In either case, for sliding (i.e., not tied) interfaces, the magnitude of P_x affects the acceleration and velocity of the upper block and should be chosen to induce motion without producing undesired inertial effects or causing the upper block to slide off of the lower block during the analysis. For tied interfaces, P_x needs only to be numerically significant as the expected interface force F_x is equal to P_x. With these considerations in mind, the chosen magnitude for the applied load in the x-direction was 3.1

units for tied and frictional interfaces and 0.31 units for frictionless interfaces. The applied load magnitudes are summarized in Table 3.

Interface Type	Load	Magnitude
All	P_y	10.0
Tied	P_x	3.1
Frictional	P_x	3.1
Frictionless	P_x	0.31

Table 3. Typical magnitudes for the applied loads.

The applied loads, P_x and P_y, are imposed by body forces in the upper block. This method of applying load is dependent only upon the material density, volume of the body, and the imposed acceleration field (e.g., gravity); therefore, the applied load is independent of the mesh discretization and can be used for all element formulations. For a given density and geometry, the acceleration magnitudes in the x- and y-directions determine P_x and P_y, respectively. The temporal variation in the applied loads is shown in Figure 3 and is controlled by specifying acceleration time histories via load curves in DYNA3D. The y-direction load is linearly ramped from zero during the first 0.1 seconds and then held constant. The x-direction load initiates at 0.3 seconds and reaches its full value at 0.4 seconds. The dwell period before the x-direction load is applied allows the transient dynamics induced by the y-direction load to decay and approach static equilibrium.

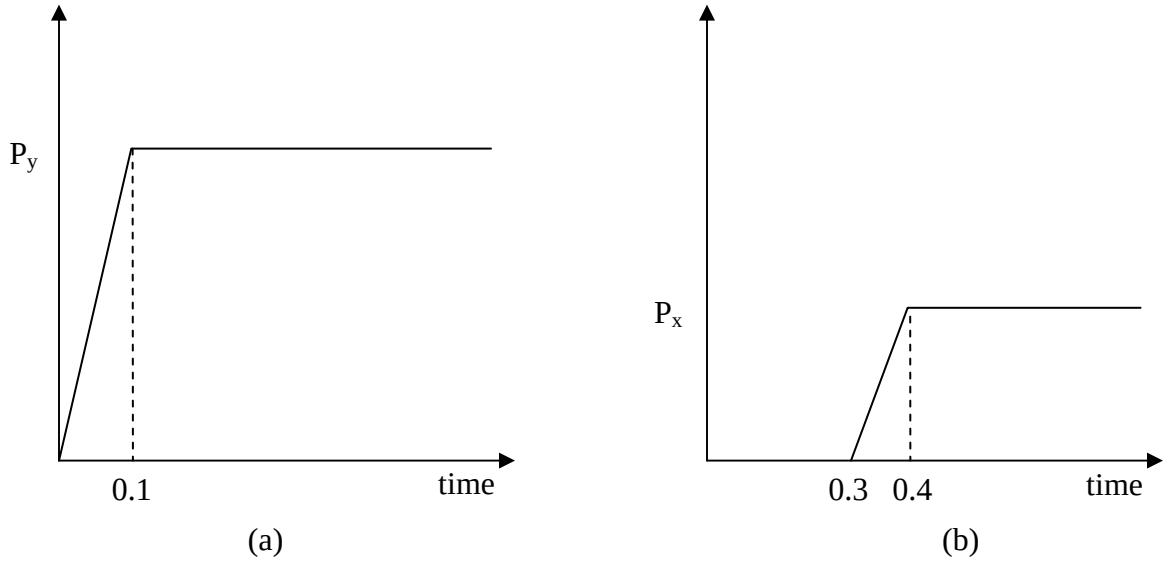

Figure 3. The loads in the y-direction (a) and the x-direction (b) are applied over a time interval of 0.1 and are held constant once their peak magnitude is reached.

3.4 MATERIAL BEHAVIOR

The material response is idealized as linear elastic. Solid elements are modeled using the hyperelastic Mooney-Rivlin (Type 27) formulation and hourglass stabilization method 10 (total displacement physical stabilization with exact volume), while the shells are represented using the

linear elastic (Type 1) material model with hourglass stabilization method 2 (Flanagan-Belytschko viscous form). The material properties were chosen for numerical convenience and are given in Table 4. The selected Mooney-Rivlin material properties result in an elastic modulus that is four times greater than the one used for the shell elements. The shell element thickness is ten percent of the block's height while the density is ten times that of the solid block. Consequently, the overall mass of the block is the same regardless of whether it is represented by solid or shell elements.

Continuum Elements Material Properties: Mooney – Rivlin (Type 27)	
Density	0.01
First Invariant Coefficient, A	909.091
Second Invariant Coefficient, B	0.0
Poisson Ratio	0.1
Hourglass Stabilization Method	10
Quadratic Bulk Viscosity Coefficient	1.5
Linear Bulk Viscosity Coefficient	0.06

Shell Elements Material Properties: Linear Elastic (Type 1)	
Density	0.1
Elastic Modulus	1000.0
Poisson Ratio	0.1
Element Formulation	2
Shell Thickness	0.1
Number of Through Thickness Gauss Integration Points	5
Hourglass Stabilization Method	2
Hourglass Stabilization Coefficient	0.1
Quadratic Bulk Viscosity Coefficient	1.5
Linear Bulk Viscosity Coefficient	0.06

Table 4. Material properties used during slide surface verification.

4 VERIFICATION CRITERIA

The verification criteria used to evaluate each contact algorithm are described along with how the data is extracted from the DYNA3D analysis. The four verification criteria are: observed deformations, nodal time histories, interface forces, and reaction forces.

4.1 OBSERVED DEFORMATIONS

The observed deformations are a gross qualitative check on the interface behavior to ensure that the nodal displacements conform to the kinematic restrictions the contact algorithm is supposed to enforce. Deformed mesh plots should reveal no apparent interpenetration along the interface, tied surfaces should remain in the same relative position, and sliding interfaces should exhibit relative motion only in the x-direction.

4.2 RELATIVE NODAL DISPLACEMENTS

Nodal time histories provide a quantitative check on the kinematic restrictions. Relative nodal displacements measure changes in the distance separating the master and slave surfaces. Negative relative y-displacements indicate interpenetration, while positive relative y-displacements indicate separation. Relative x-displacements indicate sliding along the interface. Time history results are generated using the slave and master surface nodal pairs given in Table 5 for each contact algorithm. The interface nodes are selected such that their initial position is close to the center of the contact area between the blocks.

4.3 TOTAL INTERFACE FORCE

The total interface forces acting on both the master and slave surfaces are output by DYNA3D. If the interface forces are in equilibrium, then the sum of the slave and master components should be zero in each coordinate direction (i.e., equal and opposite). It should be noted that the force balance between the master and slave surface is theoretically satisfied by both the Penalty and

	Slave Node	Master Node
Solid-on-Solid	15	77
Shell-on-Solid	91	129
Shell-on-Shell	143	181

(a) Types 1, 2, 3, 9, 10, and 12

	Slave Node	Master Node
Node-on-Solid	59	97
Node-on-Shell	7	45

(b) Types 5, 6, and 8

	Slave Node	Master Node
Node-on-Shell	3	45

(c) Type 7

Table 5. The slave and master surface nodal pairs used to generate time history results for each contact algorithm.

the Lagrange contact enforcement options. Both enforcement methods apply a force to the "master" segment that is equal and opposite as the force applied to the "slave" node. In DYNA3D, the Lagrange solver actually sums the net interface force and outputs it, sign adjusted, for both the master and slave surfaces. The magnitude and direction of the total interface forces are also compared to their expected static values. The static solution considers the interface force on the upper block; the corresponding result in the analysis is the slave surface force. The total interface force is a good quantitative measure for most contact algorithms, but not for automatic contact (Type 12). This is because automatic contact treats all interface segments as master segments and all nodes as slave nodes. As a result, the total interface force for automatic contact with penalty enforcement is always zero. When automatic contact is used with the Lagrange enforcement method, the total interface force represents the sum of the restoration forces applied to all slave nodes. However, some force cancellation may occur since segments may be oriented in opposite directions. Thus, for automatic contact, the total force reported by DYNA3D is typically lower than the actual force and is not a reliable measure.

4.4 REACTION FORCES

The reaction force associated with a prescribed boundary condition provides an indirect method for quantitatively evaluating a contact algorithm. The reaction force is output by DYNA3D and serves as a supplemental and independent check on the force transferred across the interface, i.e., the code used to calculate the reaction forces is completely independent of the contact algorithm. For the basic contact problem, static equilibrium considerations require the reaction forces to balance the interface forces, $R_x = F_x$ and $R_y = F_y$. The output reaction forces correspond to the total force exerted by the body against the support (e.g., same magnitude and direction as F_y), rather than the total force exerted by the support against the body (e.g., same magnitude but opposite direction as F_y). The DYNA3D output is consistent with the reaction forces defined for the basic contact problem in section 2. In particular, reaction forces provide a good means of evaluating automatic contact since the interface force output is not meaningful for that algorithm.

5 EXPECTED RESULTS

The expected results for each type of interface idealization are determined from the static solution developed for the generic contact problem in section 2 and the body forces and friction coefficients selected in section 3. The expected results also reflect the four verification criteria discussed in section 4.

5.1 TIED INTERFACE IDEALIZATION

The relative position of the blocks should remain unchanged for a tied interface. Therefore, the relative nodal displacements should be zero in both the x- and y-directions. The interface forces on the upper block should be equal in magnitude and opposite in direction to the applied loads. F_y should ramp linearly from zero to a peak value of 10.0 at time t = 0.1 and then remain constant. F_x should ramp linearly from zero at t = 0.3 to a peak value of -3.1 at t = 0.4 and then remain constant. The reaction forces should have the same magnitude as the interface forces, but the opposite sign. The expected interface and reaction force time histories are shown in Figure 4.

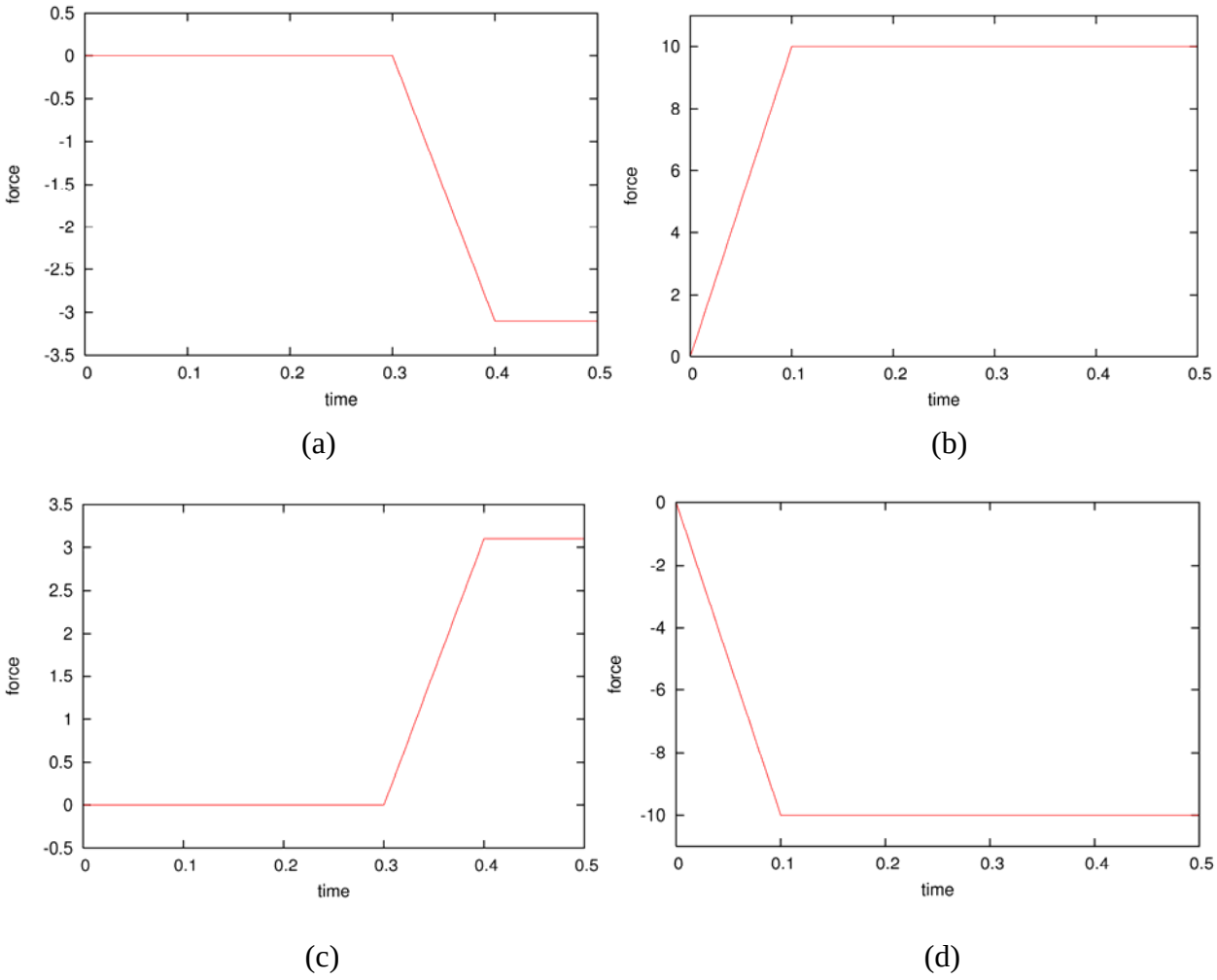

Figure 4. The expected force time histories F_x (a), F_y (b), R_x (c), and R_y (d) for the tied interface idealization.

For a tensile loading, the magnitudes of the interface and reaction forces are the same, but the signs are reversed.

5.2 FRICTIONAL INTERFACE IDEALIZATION

For frictional interfaces, the relative y-displacement between the slave and master surfaces should be zero for all time. The relative x-displacement should be zero until the body force in the x-direction exceeds f_s = 3.0, just before time t = 0.4. The upper block should then slide along the interface. F_x should be zero until t = 0.3 and then ramp linearly to a value of -3.0 near t = 0.4; it should then drop to the dynamic friction force value of -2.5. R_x should be equal and opposite of F_x. F_y and R_y should have the same magnitude and direction as the tied interface idealization. The expected interface and reaction forces time histories are given in Figure 5.

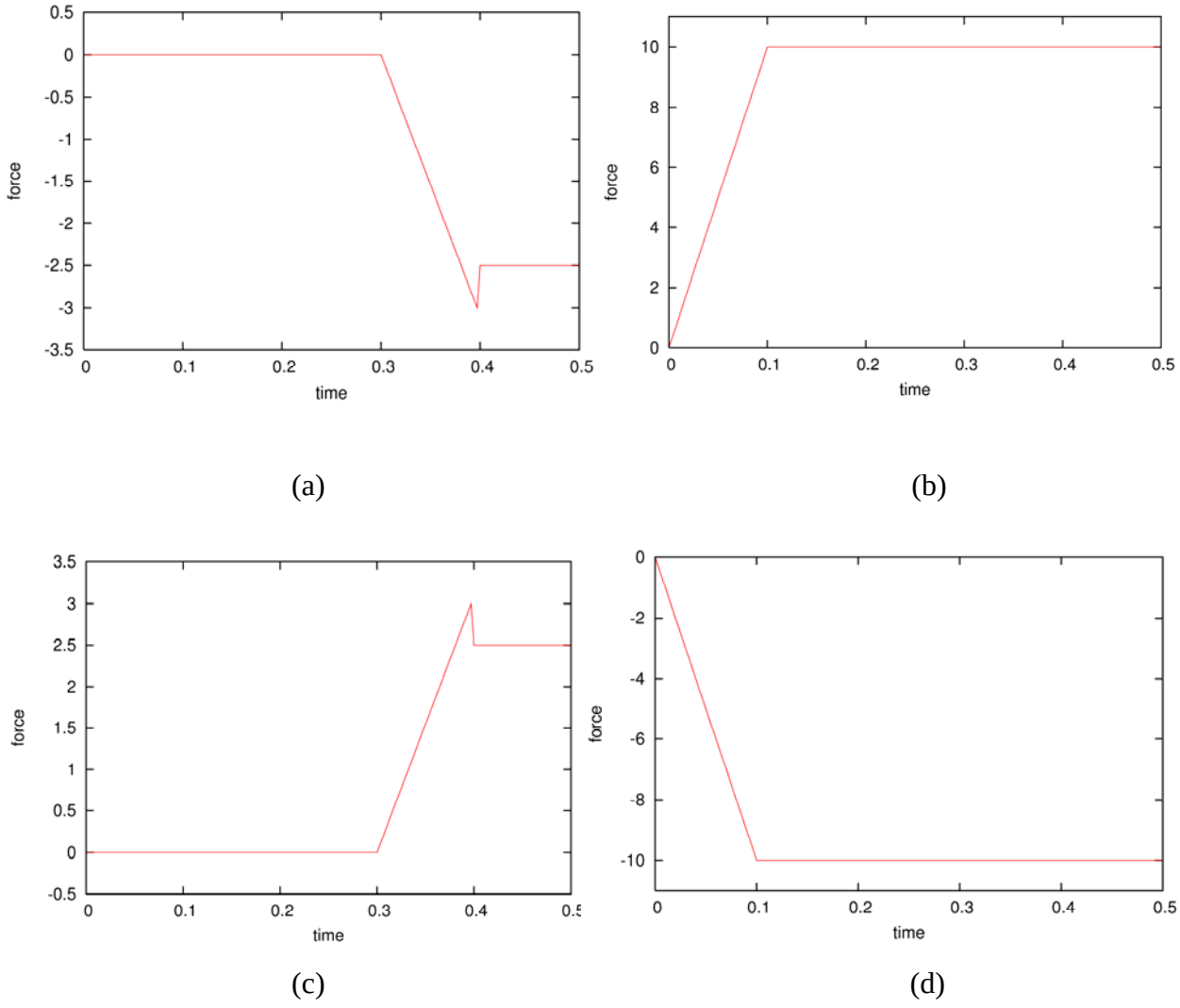

Figure 5. The expected force time histories F_x (a), F_y (b), R_x (c), and R_y (d) for the frictional interface idealization.

5.3 FRICTIONLESS INTERFACE IDEALIZATION

The frictionless interface idealization should have a relative y-displacement of zero between the slave and master surfaces for all time. Since there is no resistance to tangential movement, F_x and R_x should always be zero. F_y and R_y should have the same magnitude and direction as the tied interface idealization. The expected interface and reaction forces time histories are given in Figure 6.

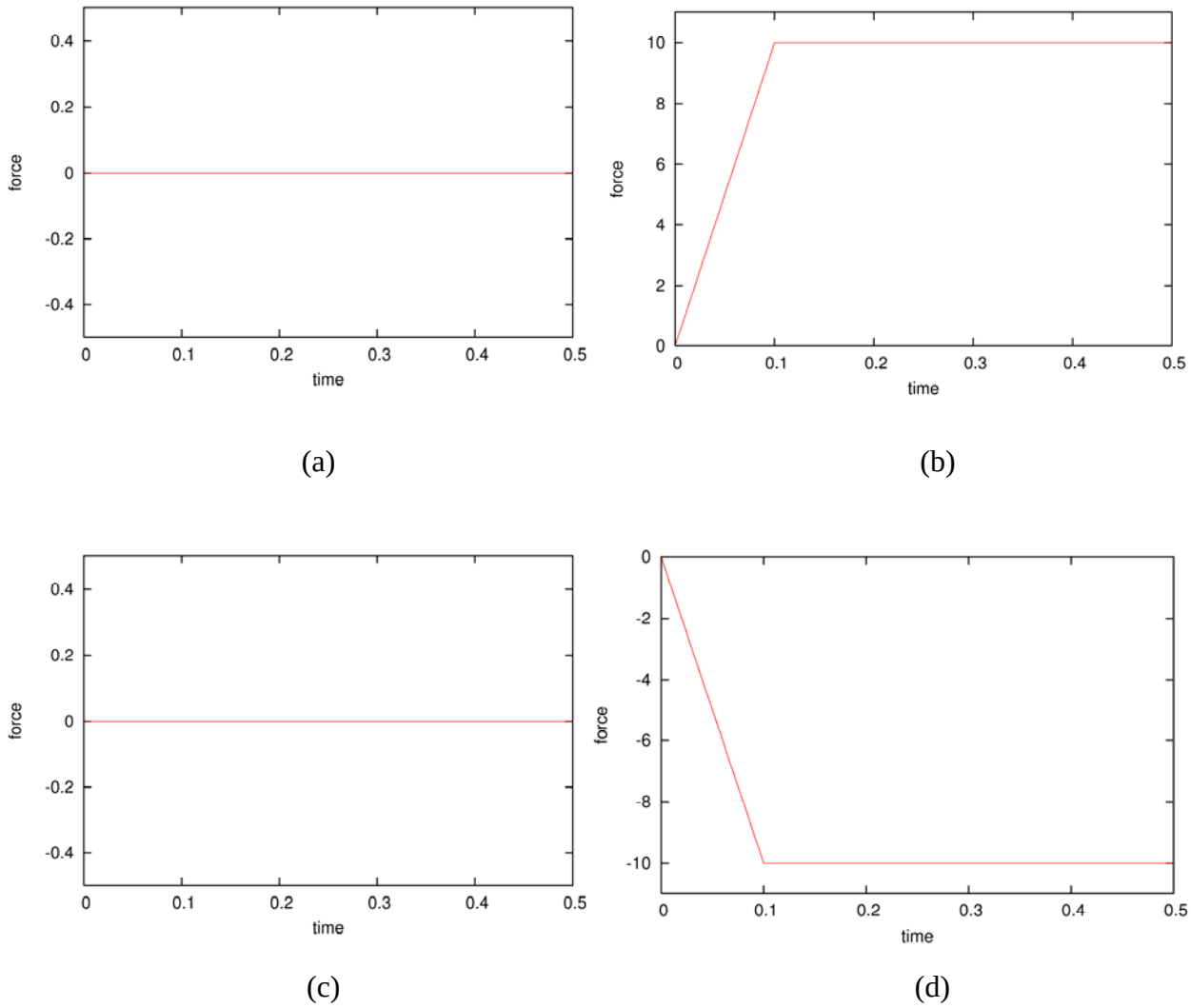

Figure 6. The expected force time histories F_x (a), F_y (b), R_x (c), and R_y (d) for the frictionless interface idealization.

5.4 FACTORS INFLUENCING THE NUMERICAL RESULTS

The DYNA3D results incorporate transient dynamic effects that are not present in the static solution. Therefore, it is expected that the analysis results will show some oscillations that should decay over time and converge to the static solution. Some contact algorithms (Types 3, 5, 8, 10, and 12) account for the shell element thickness when calculating interface interactions, either by

default or by an interface option. However, the expected interface behavior is the same whether or not the contact algorithm accounts for the shell thickness.

It was observed that the exponential decay coefficient affected the peak frictional force developed by the interface in addition to how fast the transition from static to dynamic friction occurred. As the exponential decay coefficient was increased, the observed peak friction force decreased. Since the effect on the peak friction force was more pronounced for Lagrange contact enforcement than for penalty enforcement, a smaller β is used for Lagrange contact (see Table 2). Thus, a more rounded transition from static to dynamic friction is expected for the Lagrange enforcement option compared to the penalty method.

Several contact algorithms prevent relative displacements between the slave and master surfaces until a release criterion is satisfied. For frictional interfaces, the slave and master surfaces are able to move tangentially once the static friction force is exceeded. For interfaces with a failure criterion, once the criterion is met some form of relative movement is allowed (the type of movement depends upon the interface type). The expected interface forces given in section 5 are based on a uniform (static) force distribution across the interface; this implies that all segments would satisfy the release criterion at the same time. However, in the analysis, the force distribution (i.e., element stresses) will not be completely uniform due to dynamic effects, edge effects, geometry approximations (mesh refinement), deformations (curved rather than planar contact surface), etc. The individual interface segments will not necessarily experience the same load time history, and individual segments may therefore satisfy the release criterion prior to the interface as a whole satisfying the criterion. As individual segments release, the interface's total load capacity is reduced. One potential consequence of this behavior is that sharp spikes in the expected behavior (e.g., the transition from static friction force to dynamic friction force in Figure 5 (a)) may not be resolved as precisely as the expected results. Also, since the resolution of the interface force depends upon the output interval, the peak force may occur between output states and therefore not show up on the plot. For these reasons, the general trend described in the expected results should be apparent in the numerical results; however, the numerical results are not expected to capture the spikes exactly.

Since the interface serves as the load transfer mechanism for the lower block, the interface force time history directly impacts the reaction forces generated on the lower block. Therefore, the reaction forces are likely to exhibit the same tendency as the interface force with respect to resolving the spikes.

6 CONTACT ALGORITHMS

6.1 TYPE 1: SLIDING ONLY

The sliding only contact algorithm is a single-pass, kinematic formulation that allows frictionless sliding along the master and slave surfaces, but no interpenetration or separation of the surfaces. Three types of element interaction are considered: solid-on-solid, shell-on-solid, and shell-on-shell. The body force magnitudes are P_x = 0.31 and P_y = 10.0, and the loads are applied according to the time history shown in Figure 3. The nodal time histories are generated using the nodal pairs given in Table 5(a). The expected results are discussed in section 5.3.

6.1.1 Type 1 Results

The mesh exhibits the expected deformation as the body forces are applied. The relative normal displacements are shown in Figure 7. The displacement magnitudes are close to zero, which indicates that the contact algorithm prevents interpenetration and gap formation. The total interface forces developed along the slave surface (Figure 8 (a) and (b)) correspond very well with the expected time history; however, the forces on the slave and master surfaces are not in balance. A comparison of the interface force time histories shows that the master force exceeds the slave force by as much as 31% (refer to Table 6). The excessive normal force on the master surface generates a larger than expected reaction force R_y (refer to Figure 8 (d)). The magnitude of R_x also shows oscillations that exceed F_x by two orders of magnitude. These oscillations increase over time for the shell-on-block scenario, but appear only towards the end of the analysis for the solid-on-solid and shell-on-solid scenarios. Of particular interest are the large oscillations that appear for all element interactions towards the end of the analysis (time greater than 0.45), since these oscillations occur when all loads are constant.

Element Interaction	Max. Absolute Error		
	x	y	z
Solid-on-Solid	3.0E-3	3.10	3.3E-4
Shell-on-Solid	3.6E-3	3.07	1.3E-3
Shell-on-Shell	2.9E-3	2.85	4.2E-4

Table 6. The sliding only (Type 1) master surface experiences higher forces than the slave surface, resulting in an unbalanced force transfer across the interface.

The differences between the analysis results and the expected results are primarily caused by the manner in which this kinematic algorithm enforces contact. When a slave segment and master segment are in contact, all master segment nodes are “equally” affected – even if the contact is limited to a very small portion of the master segment. In the test case, some master segments are in partial contact with the slave surface at any given time since the lower block is physically larger than the upper block. Furthermore, the particular master segments in contact with the slave surface changes as the upper block slides across the lower block. Unbalanced interface forces (with respect to master and slave surfaces) must therefore be applied to or removed from each master segment node as the segment comes into or out of contact with the slave surface. It is likely that this force transfer is a major cause of the observed interface force oscillations. The more prevalent oscillations in the shell-on-solid scenario may be due to kinematic differences in the underlying shell element formulation. There are incompatibilities in the displacement modes

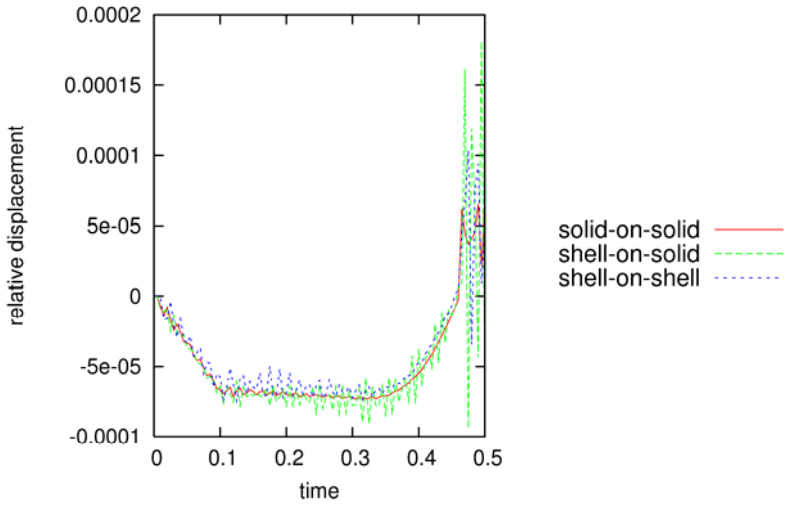

Figure 7. Relative y-displacements between the master and slave surface for the sliding only (Type 1) interface.

associated with the solid (displacement formulation, eight node linear bricks) and shell (displacement and rotation formulation, four node quadrilaterals) elements that may hinder the kinematic enforcement of sliding only contact.

6.1.2 Type 1 Summary

Overall, the sliding only interface imposes the proper constraints on relative translations, allowing tangential movement while preventing separation normal to the interface. The interface "pressure" sometimes extends too far on the master side, which results in a larger master surface force than slave force. In the test case, it was approximately 30% too high. The increased master interface force will have a varying influence on the system behavior depending upon the particular problem considered. Until the algorithm is corrected, it can be selectively deployed on a case-by-case basis that accounts for the influence of other analysis uncertainties (e.g., material properties, boundary effects, etc.). An alternative approach would be to use the Type 10 interface with the sliding only option and setting the static and dynamic coefficients of friction to zero.

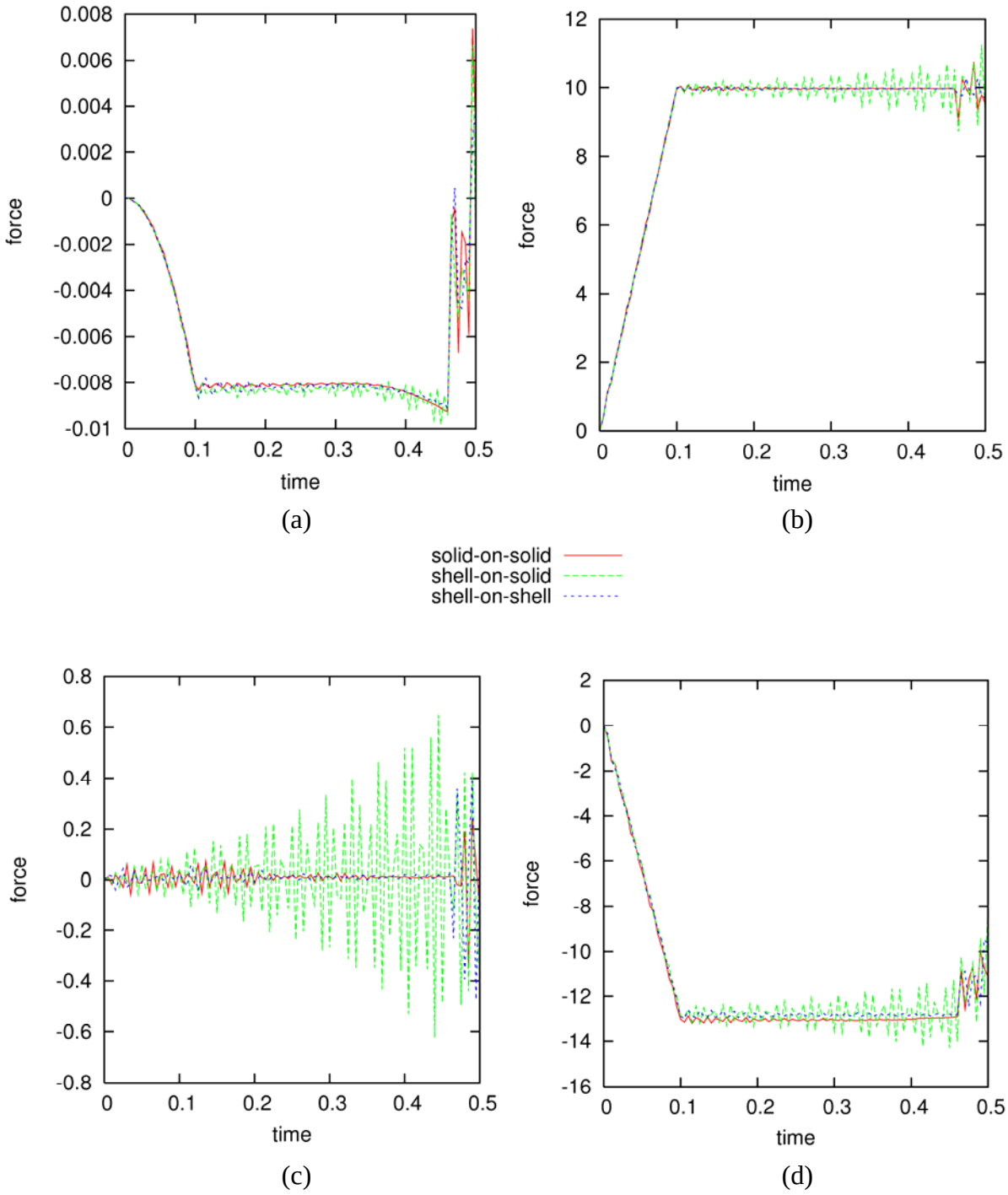

Figure 8. The interface and reaction forces for the sliding only (Type 1) interface: F_x (a), F_y (b), R_x (c), and R_y (d). The expected peak magnitudes are $F_x = R_x = 0.0$, $F_y = 10.0$, and $R_y = -10.0$.

6.2 TYPE 2: TIED

The tied contact algorithm is a single-pass, kinematic formulation that prevents relative movement of the slave and master surfaces in all coordinate directions. Three types of element interaction are considered: solid-on-solid, shell-on-solid, and shell-on-shell. Two load cases are considered to examine the behavior of the interface when the bodies are in compression and tension.

The compression load case focuses on the contact algorithm's ability to prevent interpenetration. The body force magnitudes are $P_x = 3.1$ and $P_y = 10.0$, and the loads are applied according to the time history shown in Figure 3. The tension load case focuses on preventing separation (gap formation) and checks that the contact algorithm has no directionality effects. The body forces are assigned negative magnitudes of $P_x = -3.1$ and $P_y = -10.0$ to change their direction.

For both load cases, the nodal time histories are generated using the nodal pairs given in Table 5 (a). The expected results are discussed in section 5.1.

6.2.1 Type 2 Results

The results for both load cases correspond very well to the expected behavior. The deformed mesh reflects no perceptible relative movement of the blocks over the analysis time history. This observation is confirmed by the relative nodal displacements shown in Figure 9, where the maximum relative displacement is on the order of 1.0E-4. The total interface forces and reaction forces (Figure 10 for compression and Figure 11 for tension) correspond very well to the expected time histories. The slave and master interface forces in the normal and tangential directions are in complete agreement. The total interface force in the z-direction shows a small difference between the slave and master surface. However, the forces are close to the expected value of zero, and the maximum error is only 0.04. The z-direction interface forces probably result from small differences in the upper and lower block displacements due to Poisson's effect.

6.2.2 Type 2 Summary

The tied interface preserves the relative position of the upper and lower blocks for compressive, tensile, and shear loadings. The slave and master forces are in balance and agree very well with the expected interface forces. The reaction forces on the lower block also exhibit very good agreement with the expected reaction forces.

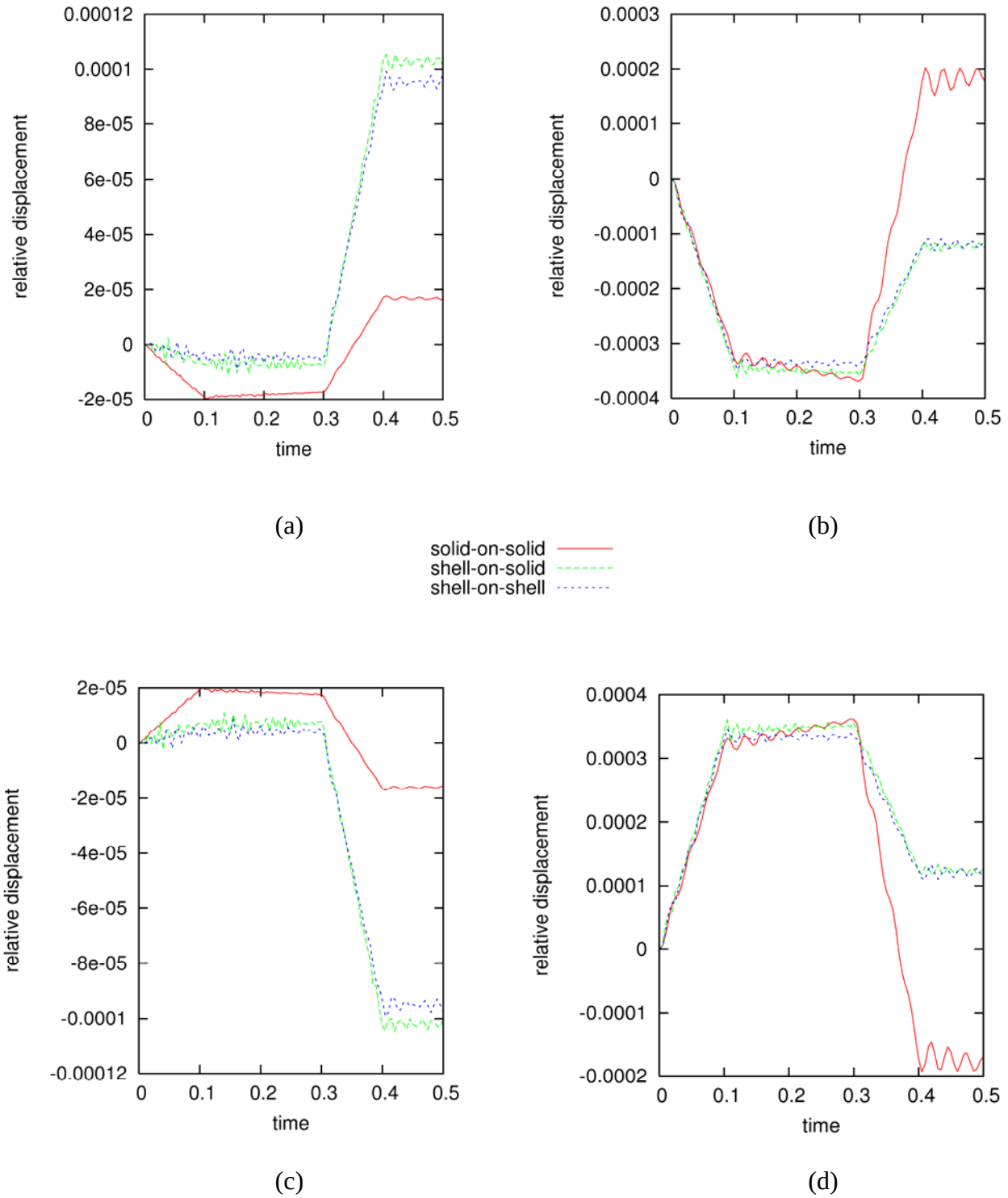

Figure 9. The relative nodal displacements between the master and slave surface of the tied (Type 2) interface are very small: the relative x-displacements (a) and y-displacements (b) during compression, and the relative x-displacements (c) and y-displacements (d) during tension.

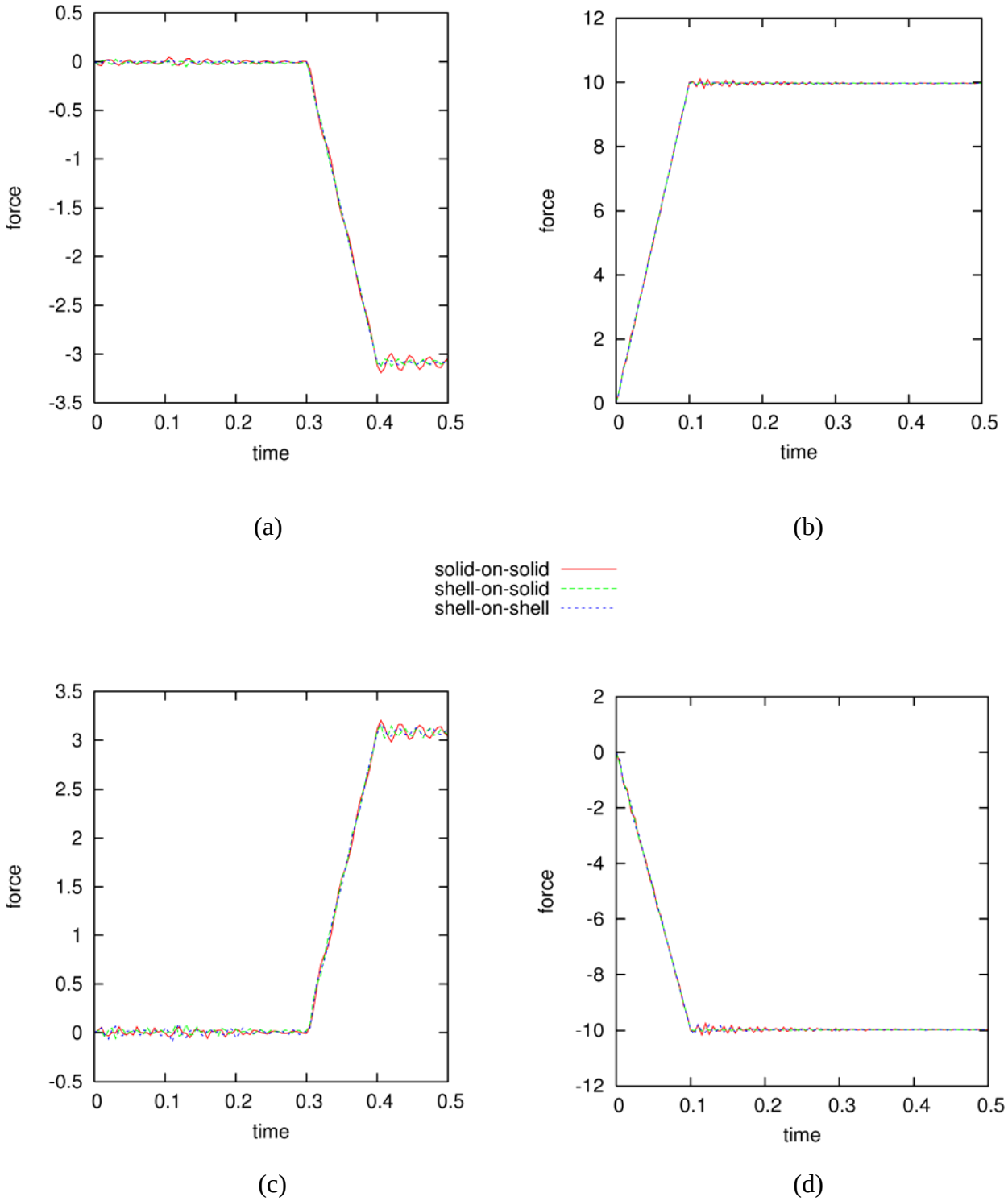

Figure 10. The interface forces, F_x (a) and F_y (b), and the total reaction forces, R_x (c) and R_y (d), for the tied (Type 2) interface during the compression load case. The expected peak magnitudes are F_x = -3.1, F_y = 10.0, R_x = 3.1, and R_y = -10.0.

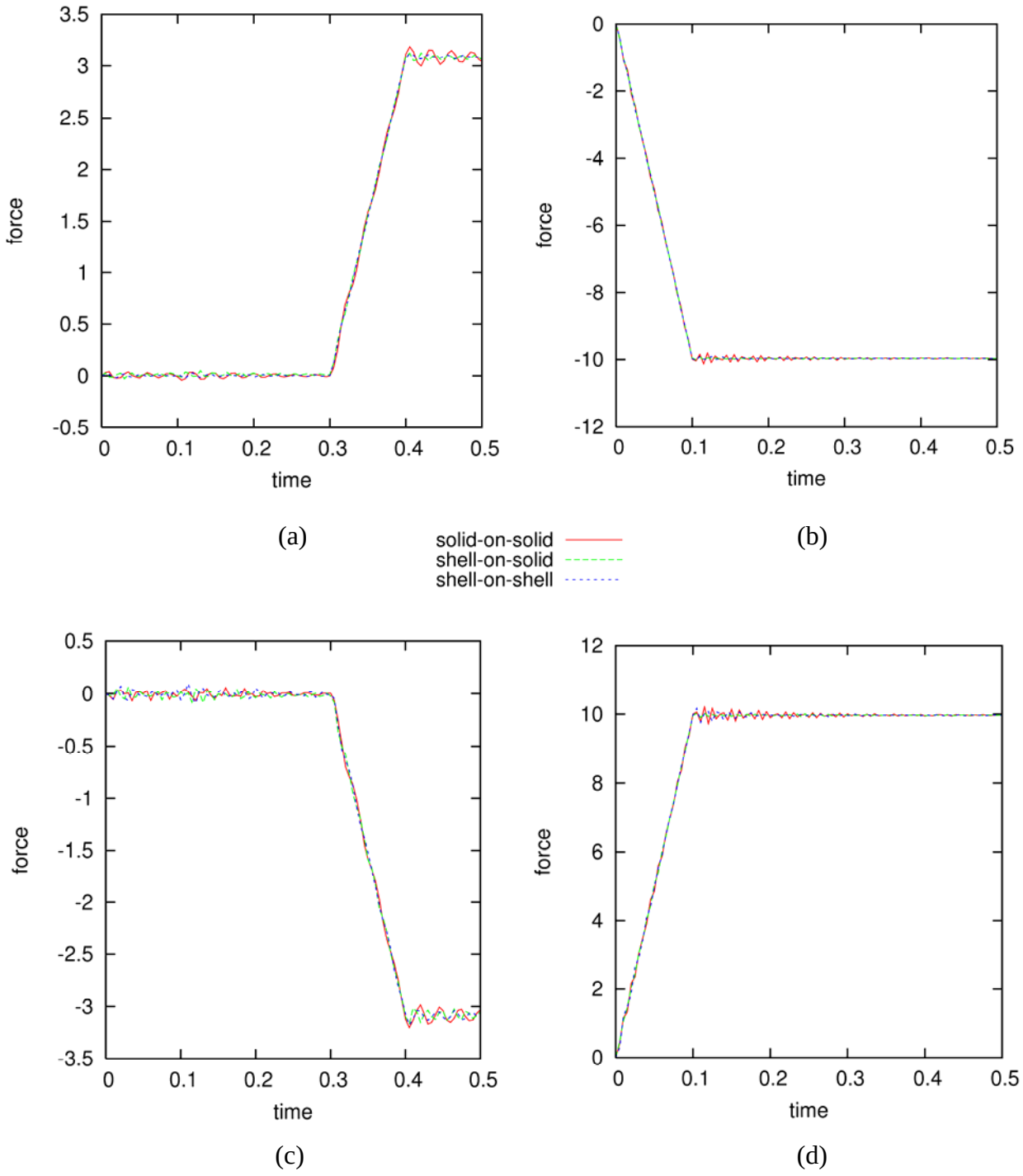

Figure 11. The interface forces, F_x (a) and F_y (b), and the total reaction forces, R_x (c) and R_y (d), for the tied (Type 2) interface during the tension load case. The expected peak magnitudes are $F_x = 3.1$, $F_y = -10.0$, $R_x = -3.1$, and $R_y = 10.0$.

6.3 TYPE 3: SLIDING WITH SEPARATION AND FRICTION

The sliding with separation and friction algorithm is a dual-pass formulation that allows bodies to form gaps and come into contact in an arbitrary manner. When portions of the slave and master surfaces are in contact, the algorithm can account for frictional forces between the surfaces and the shell element thickness. Both the penalty and Lagrange contact enforcement options are evaluated for three types of element interaction: solid-on-solid, shell-on-solid, and shell-on-shell.

The problem geometry, applied loads, and expected results are the same for both enforcement options. The body force magnitudes are P_x = 3.1 and P_y = 10.0, and the loads are applied according to the time history shown in Figure 3. The nodal time histories are generated using the nodal pairs given in Table 5 (a). The expected interface forces are discussed in section 5.2.

6.3.1 Type 3 with Penalty Enforcement

The initial penalty enforcement analysis used the default penalty stiffness factor of 1.0. The results showed significant interpenetrations (refer to Figure 12 (a) and Figure 13 (a)). For the shell-on-shell scenario, the interpenetrations approached 70% of the initial gap thickness. The interpenetrations were due, in large part, to the material properties and load magnitude selected for the test cases. The chosen material properties result in a flexible, dense block, which helps maintain a larger time-step size for the analysis. Reducing P_y would help alleviate the amount of interpenetration; however, it would also reduce the normal force that keeps the slave and master surfaces in contact and might introduce chatter as the upper block displaces. Therefore, the penalty stiffness factor was increased to reduce the interpenetration. Two additional values for the penalty stiffness factor were considered: 10.0 and 100.0. Increasing the penalty stiffness factor greatly reduced the observed penetrations (refer to Figure 12 and Figure 13); however, it also reduced the time-step size for the analysis (Table 7). The interface forces generated for each penalty stiffness factor were similar. The only significant variation was the introduction of some fairly large interface force oscillations for the shell-on-block scenario (Figure 14) when the penalty stiffness factor was 100.0. Based on these results, a penalty stiffness factor of 10.0 is used to assess the contact behavior with penalty enforcement.

Penalty Stiffness Factor	Analysis Time Step Size
1.0	4.17E-04
10.0	3.05E-04
100.0	5.35E-05

Table 7. Increasing the penalty stiffness factor to eliminate interpenetration resulted in a smaller analysis time-step size.

The mesh deformations match the expected behavior. The relative normal displacements are prevented fairly well. The maximum interpenetration observed for the solid-on-solid and shell-on-solid scenarios is on the order of 1E-03, while the shell-on-shell scenario exhibits a slightly larger interpenetration on the order of 7E-03 (or approximately 7% of the initial gap thickness). The total interface forces (Figure 15) show excellent agreement with the expected normal and frictional forces. The peak friction force for the solid-on-solid scenario is 2.95 (98% of the

theoretical peak), while the peak magnitude developed by the shell-on-solid and shell-on-shell scenarios is 2.90 (97% of the theoretical peak). The transition from static to dynamic friction is also resolved very well, with only a slight rounding due to the exponential friction law in DYNA3D. The reaction forces show a little more dynamic oscillation than the interface forces, but they still correspond very well to the expected time histories. The slave and master forces are balanced in all three coordinate directions.

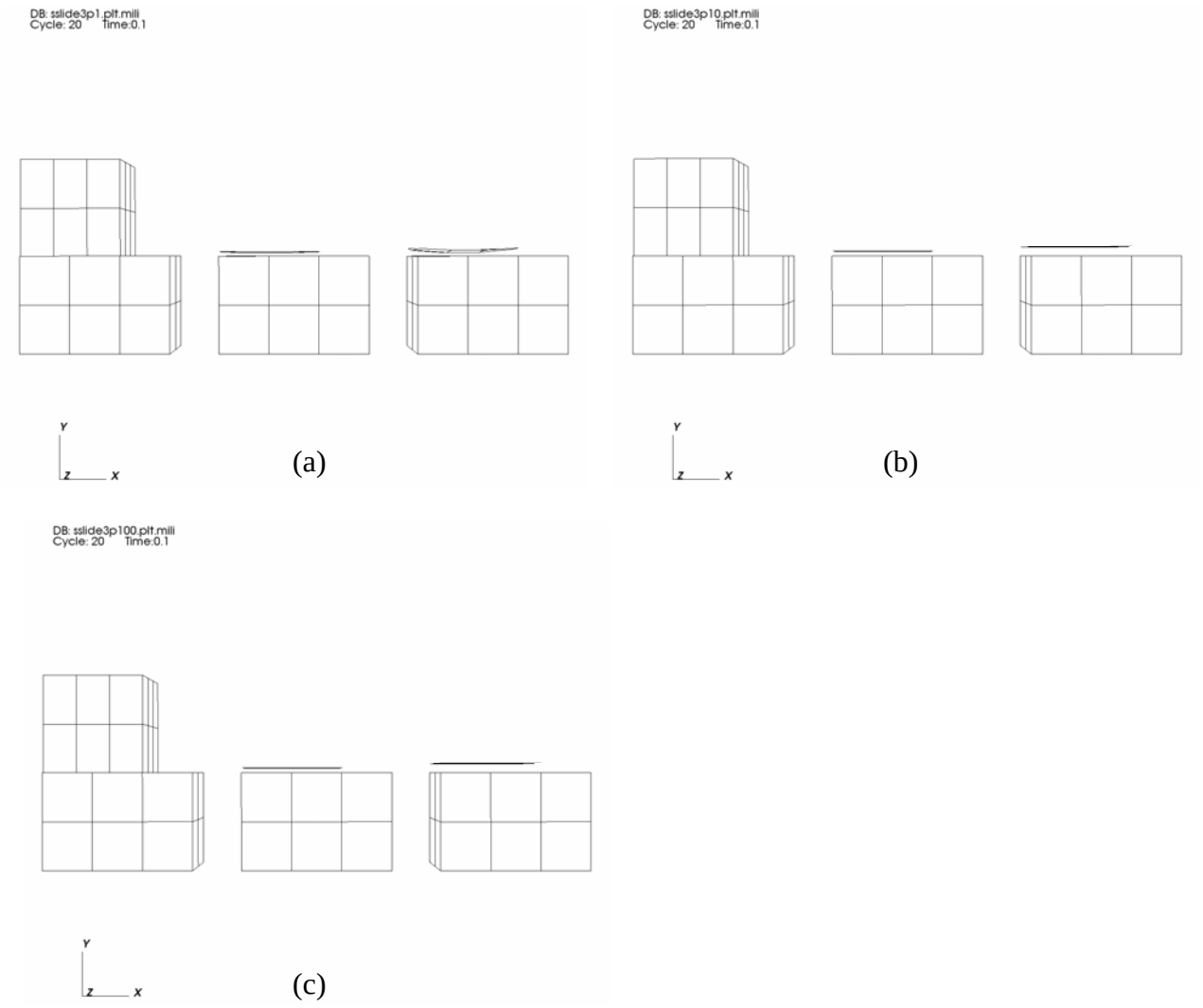

Figure 12. The penalty stiffness factor influences interpenetrations along the sliding with separation and friction (Type 3) interface. The penalty stiffness scale factors are: 1.0 (a), 10.0 (b), and 100.0 (c).

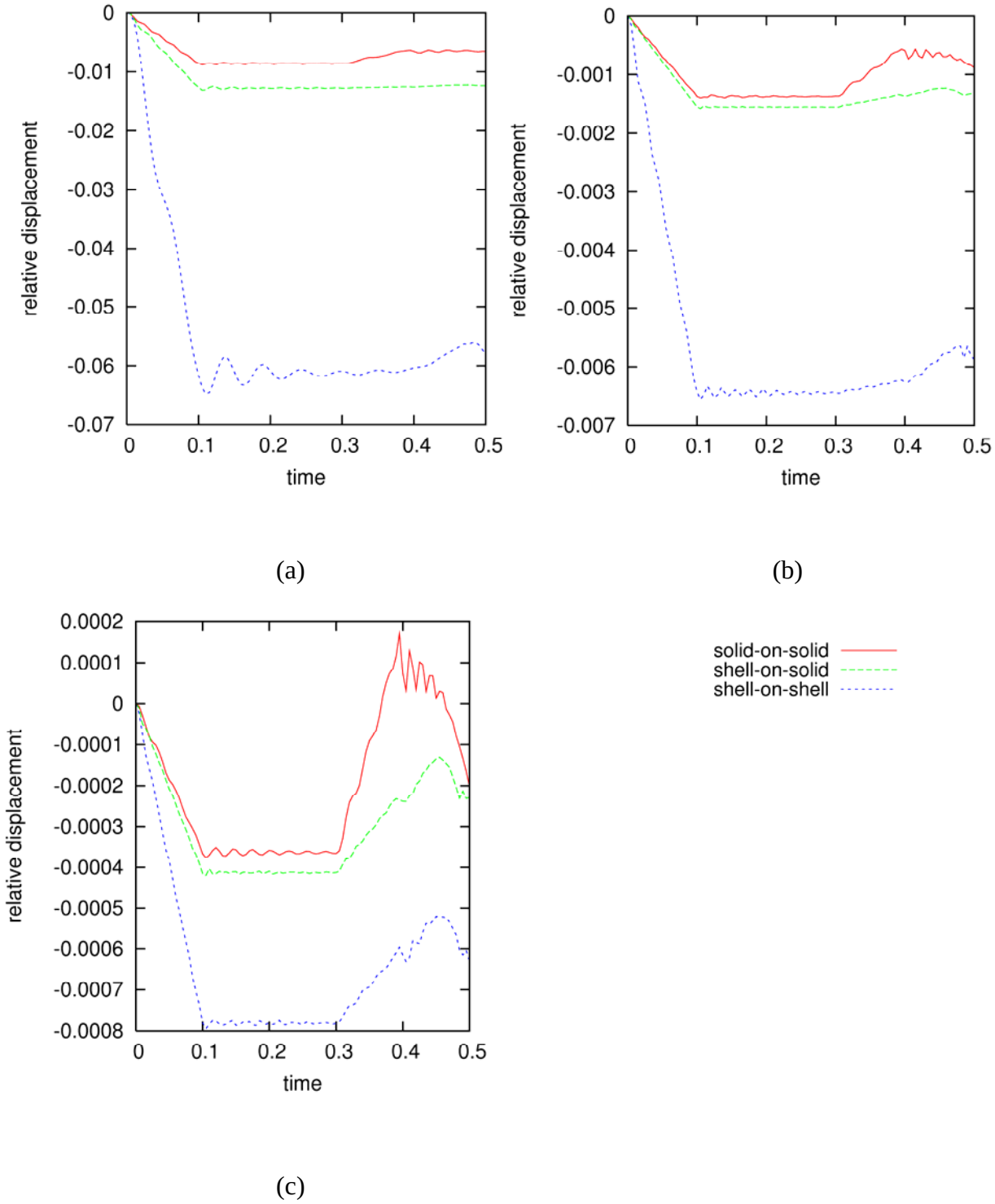

Figure 13. Relative y-displacements indicate the amount of interpenetration along the sliding with separation and friction (Type 3) interface for penalty stiffness scale factors of 1.0 (a), 10.0 (b), and 100.0 (c).

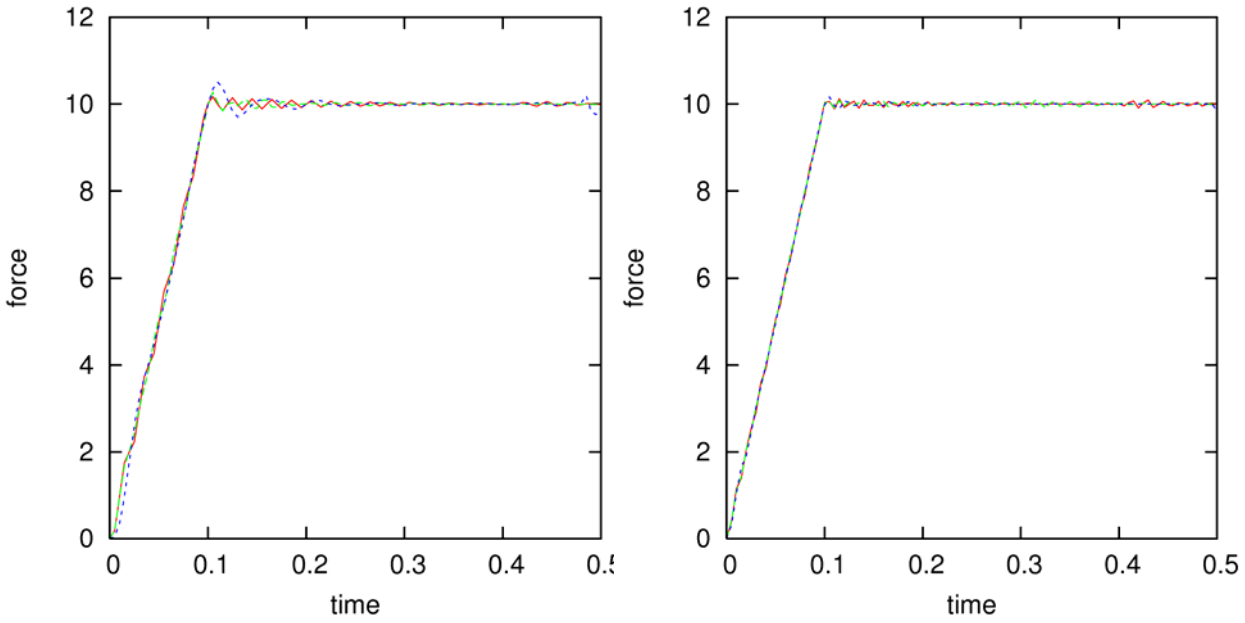

(a)

(b)

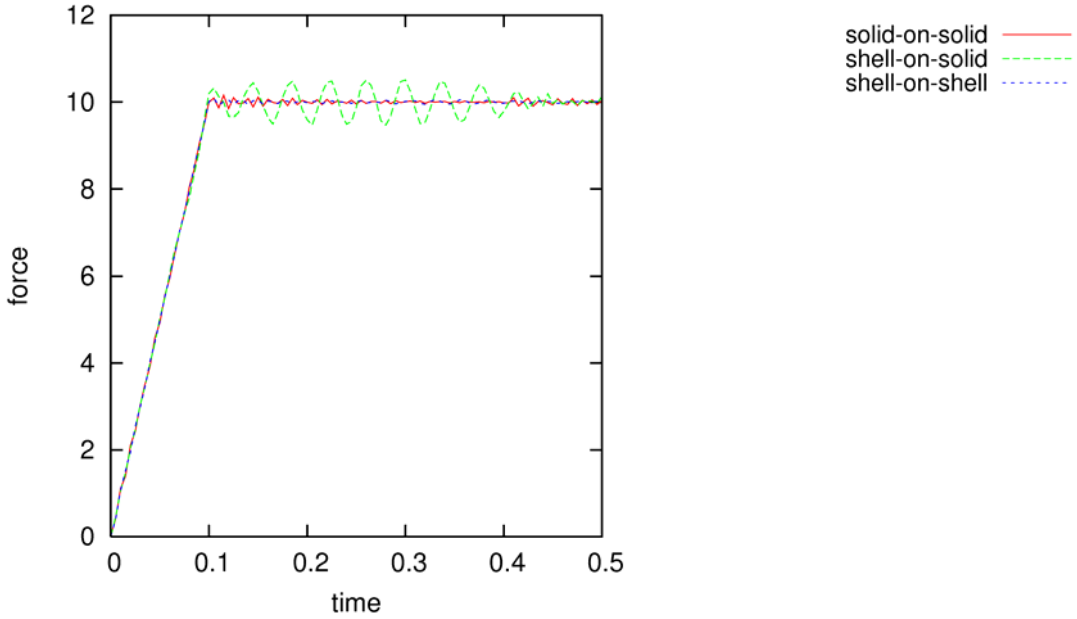

(c)

Figure 14. The normal interface forces developed along the sliding with separation and friction (Type 3) interface were very similar for penalty stiffness factors of 1.0 (a), 10.0 (b), and 100.0 (c) when using the penalty enforcement option.

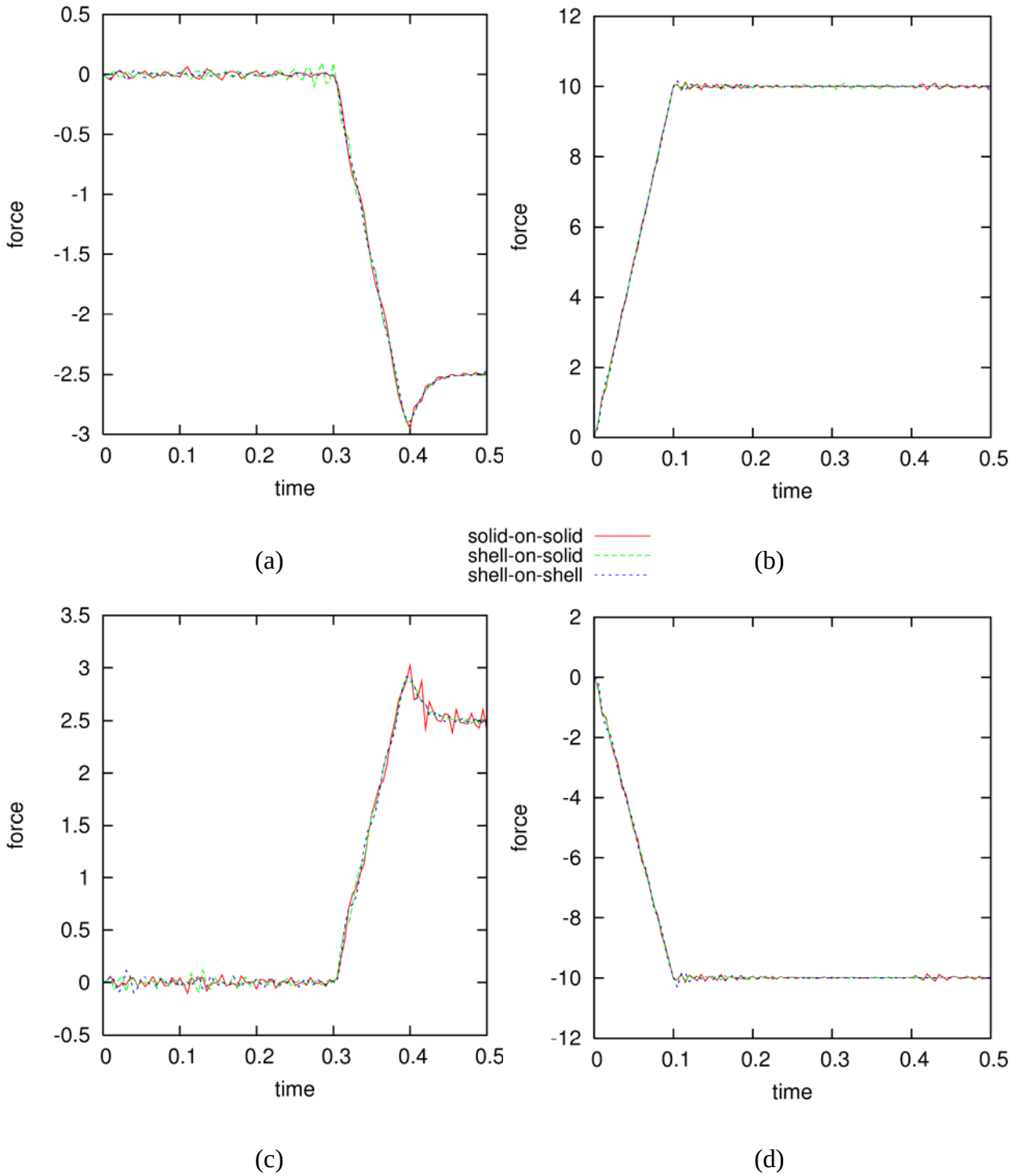

Figure 15. The total interface forces F_x (a) and F_y (b) and the total reaction forces R_x (c) and R_y (d) for the sliding with separation and friction (Type 3) interface and a penalty stiffness factor of 10.0. The expected friction forces are f_s = 3.0 and f_k = 2.5, and the expected peak normal forces are F_y = 10.0 and R_y = -10.0.

6.3.2 Type 3 with Lagrange Enforcement

The mesh deformations reveal no apparent relative displacements in the normal direction. Nodal time histories show a maximum interpenetration (Figure 16) of approximately 3E-04, which occurs for the solid-on-solid scenario. The total interface forces (Figure 17 (a) and (b)) show very good agreement with the expected normal and frictional forces, except for a couple of details. In the solid-on-solid scenario, the total interface force does not capture the additional frictional resistance that the static friction force has above the kinetic friction force. The peak friction force is approximately 2.6 (87% of the theoretical peak) for the solid-on-solid scenario, compared to 2.81 (94% of the theoretical peak) for the shell-on-solid and 2.74 (91% of the theoretical peak) for the shell-on-shell scenarios. Additionally, in all the interaction scenarios, the interface force has a rounded transition from static to dynamic friction rather than a sharp spike. The generated reaction forces (Figure 17 (c) and (d)) match the total interface force time histories very well.

6.3.3 Type 3 Summary

The sliding with separation and friction interface provides a very general capability to model the interaction between bodies. Both the penalty and Lagrange enforcement options performed very well in most respects. The penalty option can be sensitive to the penalty stiffness factor and may need to be adjusted for some problems. The Lagrange option is more effective at preventing interpenetration, but wasn't able to resolve peak friction force or the transition from static to kinetic friction as well as the penalty method. Although either enforcement option works fine in many problems, the Lagrange formulation is more robust, is not dependent on the specification of a "stiffness factor", and does not affect the analysis time-step size.

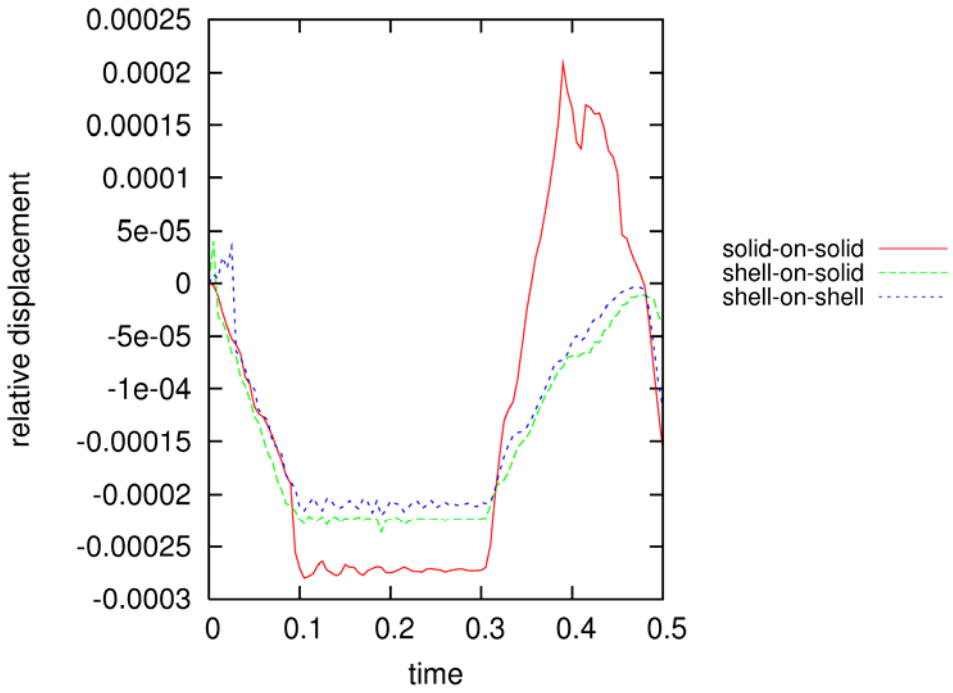

Figure 16. The Lagrange enforcement option keeps the relative y-displacements between the master and slave surface very small for the sliding with separation and friction (Type 3) interface.

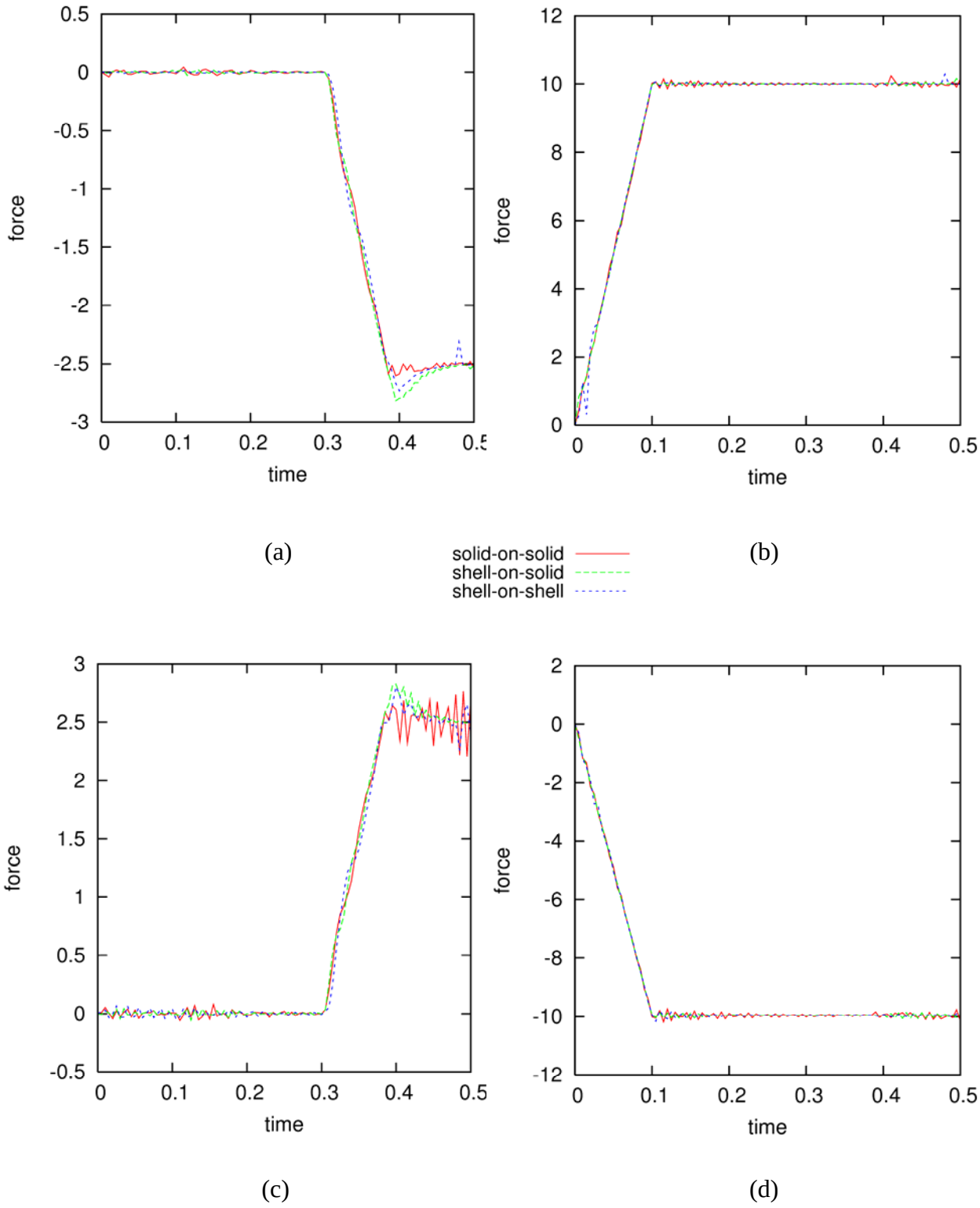

Figure 17. The total interface forces F_x (a) and F_y (b) and the total reaction forces R_x (c) and R_y (d) developed on the sliding with separation and friction (Type 3) interface using the Lagrange enforcement option. The expected friction forces are f_s = 3.0 and f_k = 2.5, and the expected peak normal forces are F_y = 10.0 and R_y = -10.0.

6.4 TYPE 5: DISCRETE NODES IMPACTING A SURFACE

The discrete nodes impacting a surface algorithm is a single-pass formulation that allows frictional contact and void formation along the interface. The slave surface is defined in terms of slave nodes (rather than segments) with an optional radius to account for thickness effects. Additionally, the master surface can account for shell element thickness. Contact occurs when the distance between the slave node and the master surface is less than the radius. Both the penalty and Lagrange contact enforcement options are evaluated for two types of element interaction: node-on-solid and node-on-shell.

The slave node radius is set to one-half of the shell element thickness, and the shell element thickness is accounted for along the master surface. Based upon the penalty enforcement results for the Type 3 interface, a penalty stiffness factor of 10.0 is used to prevent large interpenetrations. The problem geometry, applied loads, and expected results are the same for both enforcement options. The body force magnitudes are $P_x = 3.1$ and $P_y = 10.0$, and the loads are applied according to the time history shown in Figure 3. The nodal time histories are generated using the nodal pairs given in Table 5 (b). The expected interface forces are discussed in section 5.2.

6.4.1 Type 5 with Penalty Enforcement

The mesh deformations correspond very well to the expected behavior. The relative normal displacements are prevented fairly well (Figure 18). The maximum interpenetration observed for the node-on-solid scenarios is on the order of 1E-03, while the node-on-shell scenario exhibits a slightly larger interpenetration on the order of 8E-03 (or approximately 8% of the initial gap thickness). The total interface forces (Figure 19 (a) and (b)) agree very well with the expected normal and frictional forces. The peak friction force is captured well for both scenarios (2.88 for node-on-shell and 2.85 for node-on-solid), and the transition from static to dynamic friction is only slightly rounded. The reaction forces (Figure 19 (c) and (d)) show a little more dynamic oscillation than the interface forces, but they still correspond very well to the expected time histories. The slave and master forces are balanced in all three coordinate directions.

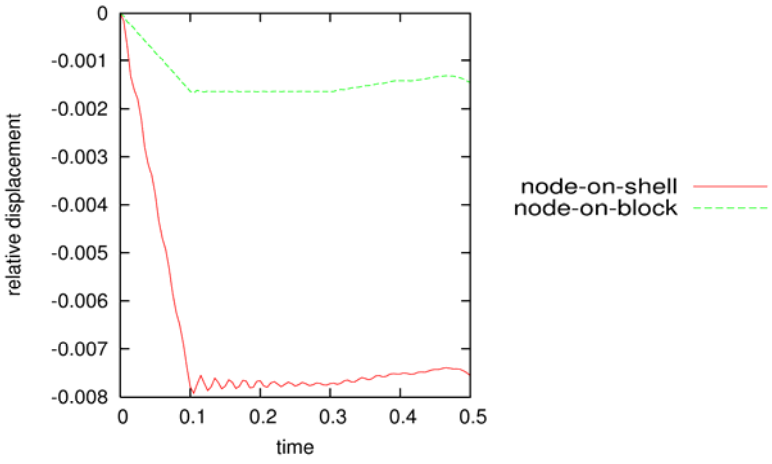

Figure 18. The relative y-displacements show that the penalty enforcement option controls interpenetration fairly well with a penalty stiffness factor of 10.0 for the discrete nodes impacting a surface (Type 5) interface.

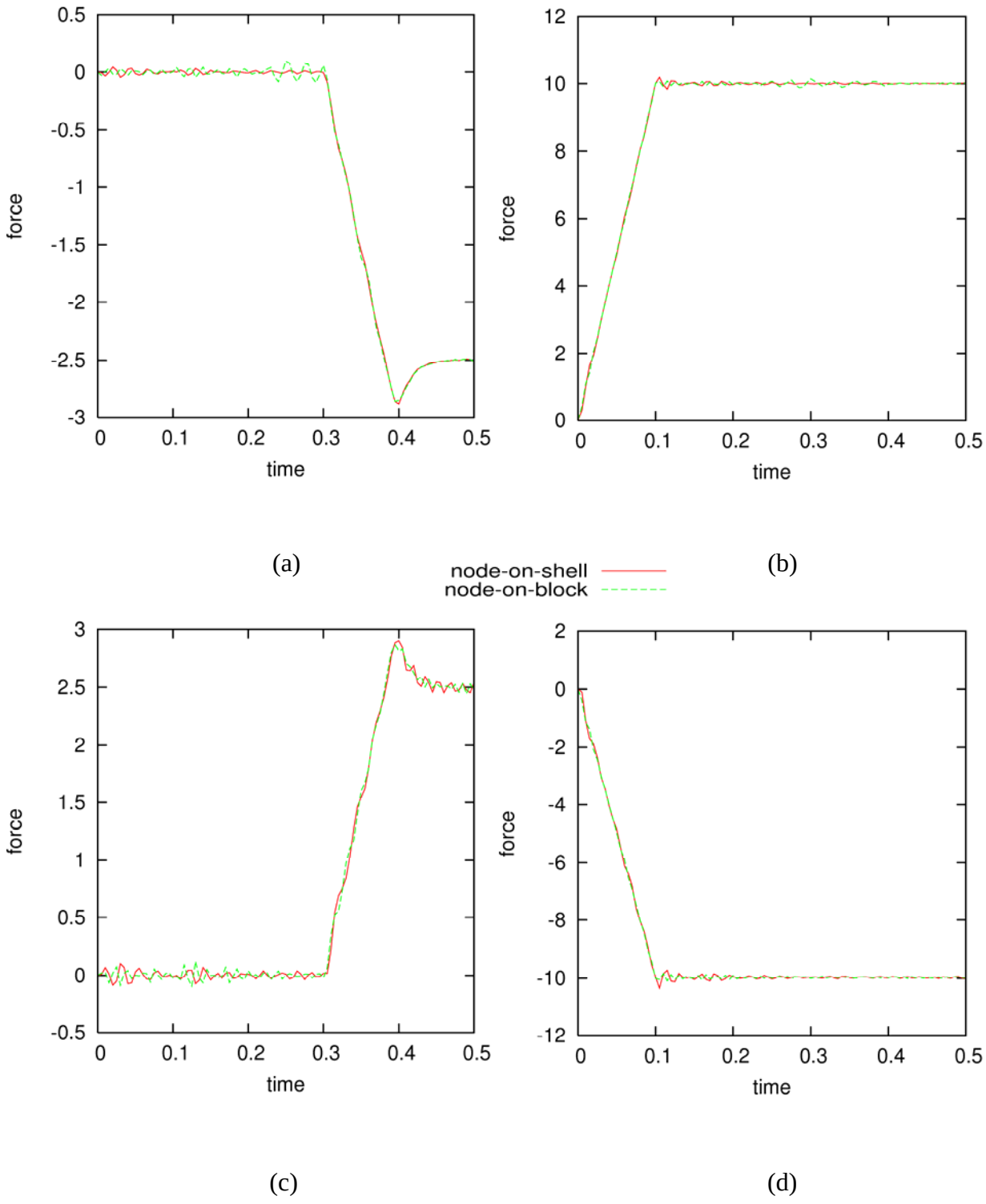

Figure 19. The interface forces, F_x (a) and F_y (b), and the reaction forces, R_x (c) and R_y (d), developed using the penalty enforcement option for the discrete nodes impacting a surface (Type 5) interface. The expected friction forces are f_s = 3.0 and f_k = 2.5, and the expected peak normal forces are F_y = 10.0 and R_y = -10.0.

6.4.2 Type 5 with Lagrange Enforcement

The mesh deformations match the expected behavior. The maximum interpenetration observed (Figure 20) is approximately 3.5E-04. The total interface forces (Figure 21 (a) and (b)) show very good agreement with the expected normal and frictional forces, although there are a few differences from the expected results. The peak friction force is captured a little better in the node-on-solid scenario (2.88) than the node-on-shell scenario (2.72). Also, the interface force has a rounded transition from static to dynamic friction rather than a sharp spike. The generated reaction forces (Figure 21 (c) and (d)) match the total interface force time histories very well.

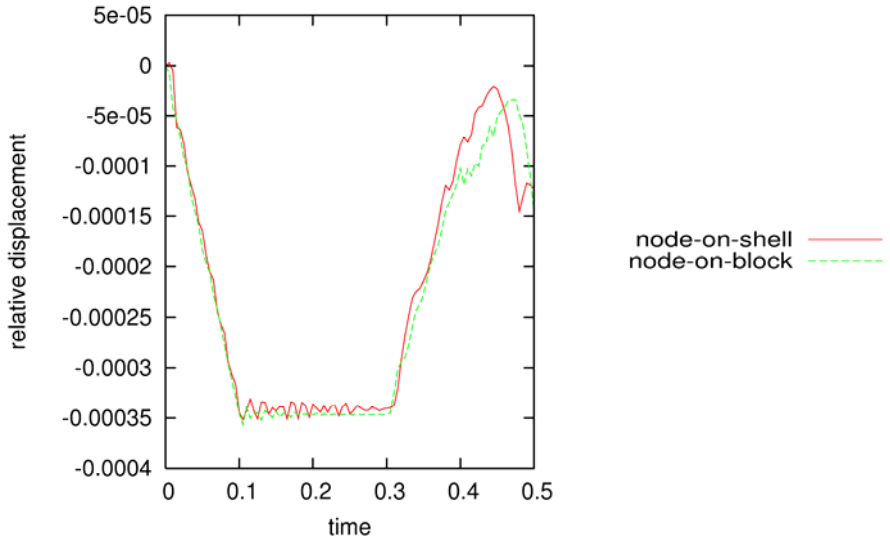

Figure 20. The relative y-displacements show that the Lagrange enforcement option keeps the interpenetrations very small for the discrete nodes impacting a surface (Type 5) interface.

6.4.3 Type 5 Summary

The discrete nodes impacting a surface interface provides a very general capability to model the interaction between beams and shell edges with solid and shell surfaces. Both the penalty and Lagrange enforcement options performed very well in most respects. The penalty option can be sensitive to the penalty stiffness factor, and may need to be adjusted for some problems. The Lagrange option is more effective at preventing interpenetration, but wasn't able to resolve the transition from static to kinetic friction as well as the penalty method. Although either enforcement option works fine for many problems, the Lagrange formulation is more robust, is not dependent on the specification of a "stiffness factor", and does not affect the analysis time-step size.

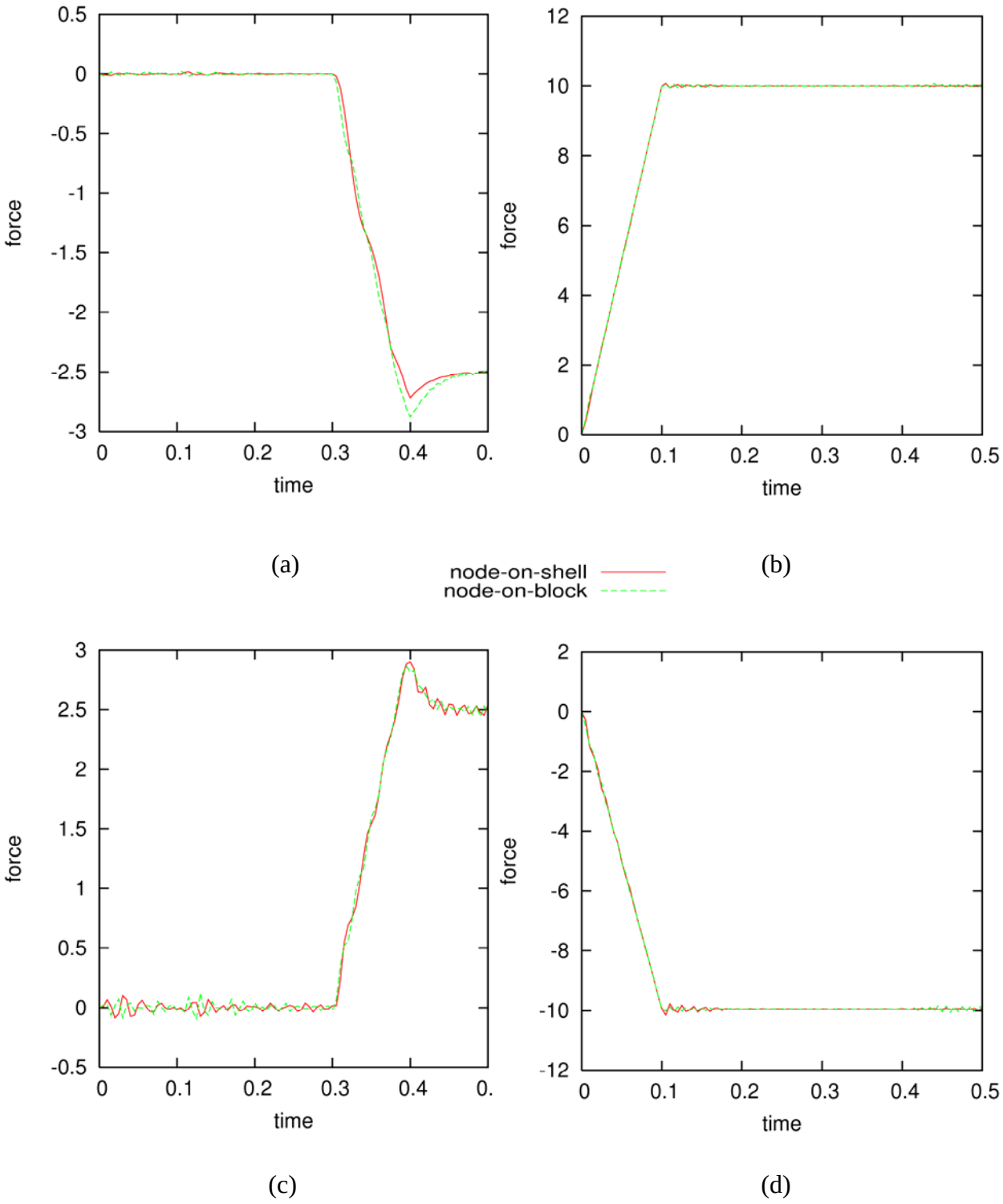

Figure 21. The interface forces, F_x (a) and F_y (b), and the reaction forces, R_x (c) and R_y (d), developed using the Lagrange enforcement option for the discrete nodes impacting a surface (Type 5) interface. The expected friction forces are $f_s = 3.0$ and $f_k = 2.5$, and the expected peak normal forces are $F_y = 10.0$ and $R_y = -10.0$.

6.5 TYPE 6: DISCRETE NODES TIED TO A SURFACE

The discrete nodes tied to a surface algorithm is a single-pass, kinematic formulation that prevents relative movement of the slave and master surfaces in all coordinate directions. The slave surface is defined in terms of slave nodes (rather than segments). Node-on-solid and node-on-shell element interactions are considered.

A tensile load is applied according to the time history shown in Figure 3 using body force magnitudes of P_x = 3.1 and P_y = -10.0. The nodal time histories are generated using the nodal pairs given in Table 5 (b). The expected interface forces are discussed in section 5.1.

6.5.1 Type 6 Results

The mesh deformations correspond very well to the expected behavior. Relative displacements are prevented very well in both the x- and y-directions (Figure 22). The maximum observed relative x-displacement is approximately 1E-04, while the maximum observed relative y-displacement is approximately 3.5E-04. The total interface forces (Figure 23 (a) and (b)) agree very well with the expected normal and tangential forces. The reaction forces (Figure 23 (c) and (d)) also show very good agreement with the expected time histories. The slave and master forces are balanced in all three coordinate directions.

6.5.2 Type 6 Summary

The discrete nodes tied to a surface interface provides a very effective capability to model beams and shell edges tied to solid and shell surfaces. The kinematic enforcement algorithm does a very good job of preventing relative displacements, and the interface forces are resolved very well.

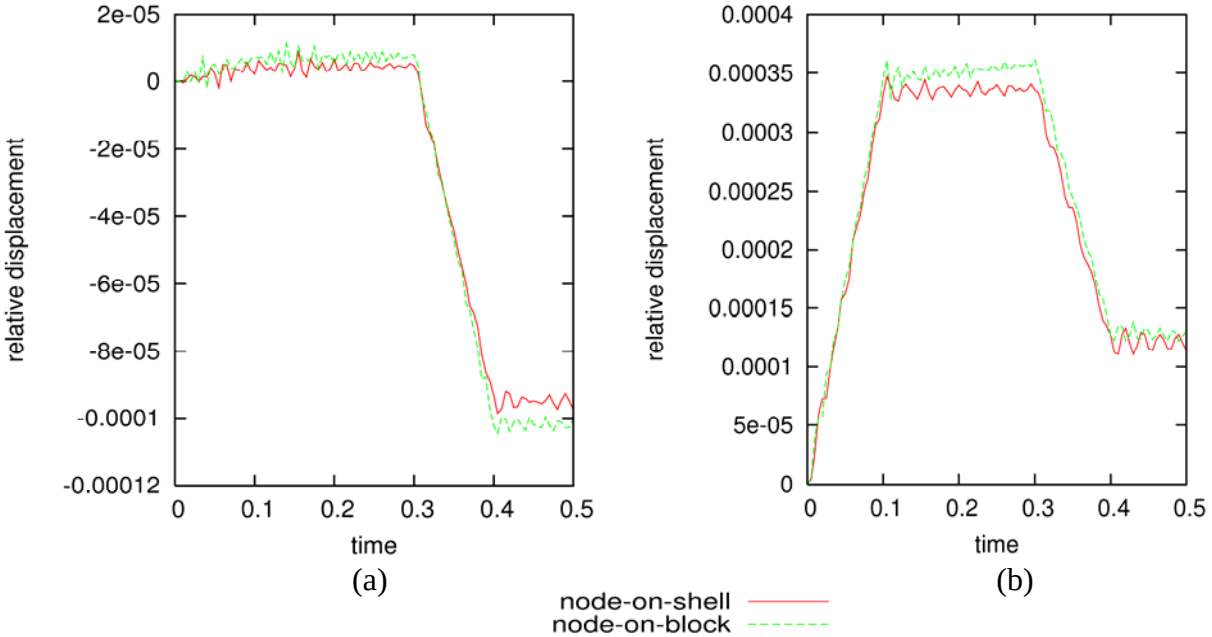

Figure 22. The kinematic enforcement option prevents relative displacements in the x-direction (a) and the y-direction (b) very well for the discrete nodes tied to a surface (Type 6) interface.

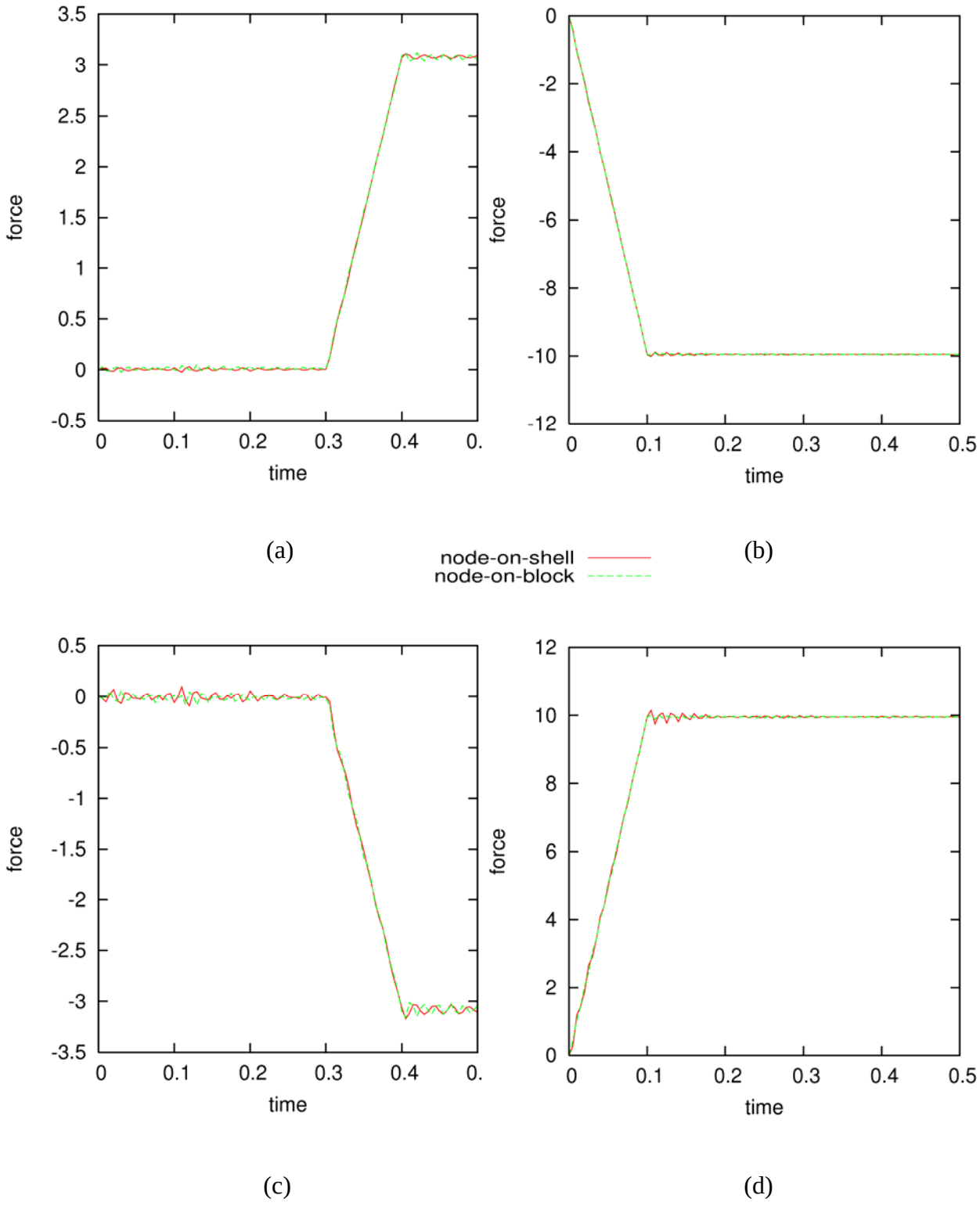

Figure 23. The interface forces, F_x (a) and F_y (b), correspond very well to the expected maximum forces of $F_x = 3.1$ and $F_y = -10$. The reaction forces, R_x (c) and R_y (d), match the interface forces very well for the discrete nodes tied to a surface (Type 6) interface.

6.6 TYPE 7: SHELL EDGE TIED TO A SHELL SURFACE

The shell edge tied to a shell surface is a specialized interface that prevents relative movement in all coordinate directions. The algorithm is a single-pass, kinematic formulation for node-on-shell interaction.

For this case, the shell elements representing the upper body are oriented in the y-z plane (see Figure 24). A pure tensile load is applied according to the time history shown in Figure 3 (a) using a body force magnitude of P_y = -10.0. Application of a body force in the x-direction would induce rotation of the upper body about the tied shell edge and was therefore avoided (P_x = 0). The nodal time histories are generated using the nodal pairs given in Table 5 (c). The expected interface force in the x-direction is zero and the expected interface force in the y-direction corresponds to the description of F_y in section 5.1.

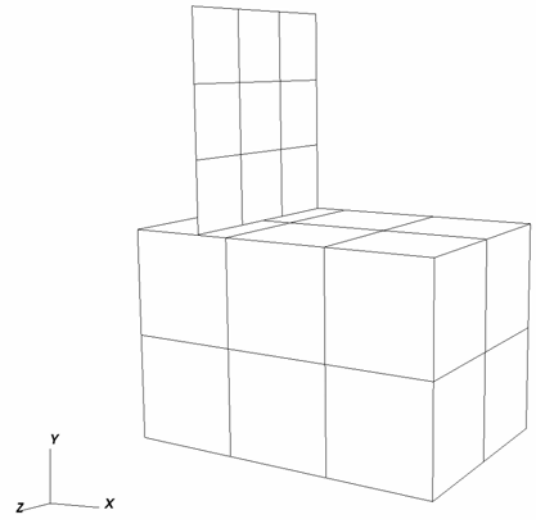

Figure 24. For the Type 7 interface verification, the upper body is represented using shell elements oriented in the y-z plane.

6.6.1 Type 7 Results

The mesh deformations match the expected behavior. Relative displacements are prevented very well in both the x- and y-directions (Figure 22). The maximum observed relative x-displacement is less than 1E-04, while the maximum observed relative y-displacement is approximately 4.5E-04. The total interface force and the reaction force in the x-direction (Figure 25 (a) and (c)) are very close to zero. The total interface force and the reaction force in the y-direction exhibit some decaying oscillations about the peak force due to dynamic effects, but otherwise agree very well with the expected forces F_y and R_y. The slave and master forces are balanced in all three coordinate directions.

6.6.2 Type 7 Summary

The intersection between a shell edge and a shell surface is effectively represented by the Type 7 interface when the mesh discretization prevents merging nodes. The kinematic enforcement algorithm does a very good job of preventing relative displacements, and the interface forces are resolved very well.

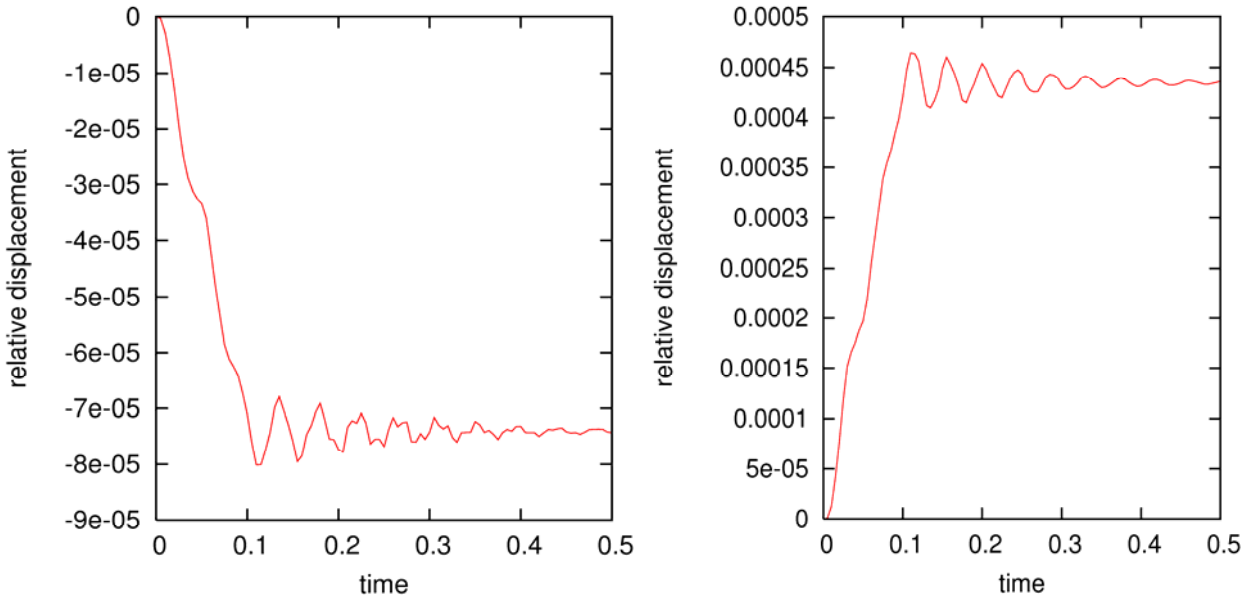

(a) (b)

Figure 25. The kinematic enforcement option prevents relative displacements in the (a) x-direction (a) and the y-direction (b) very well for the shell edge tied to a shell surface (Type 7) interface.

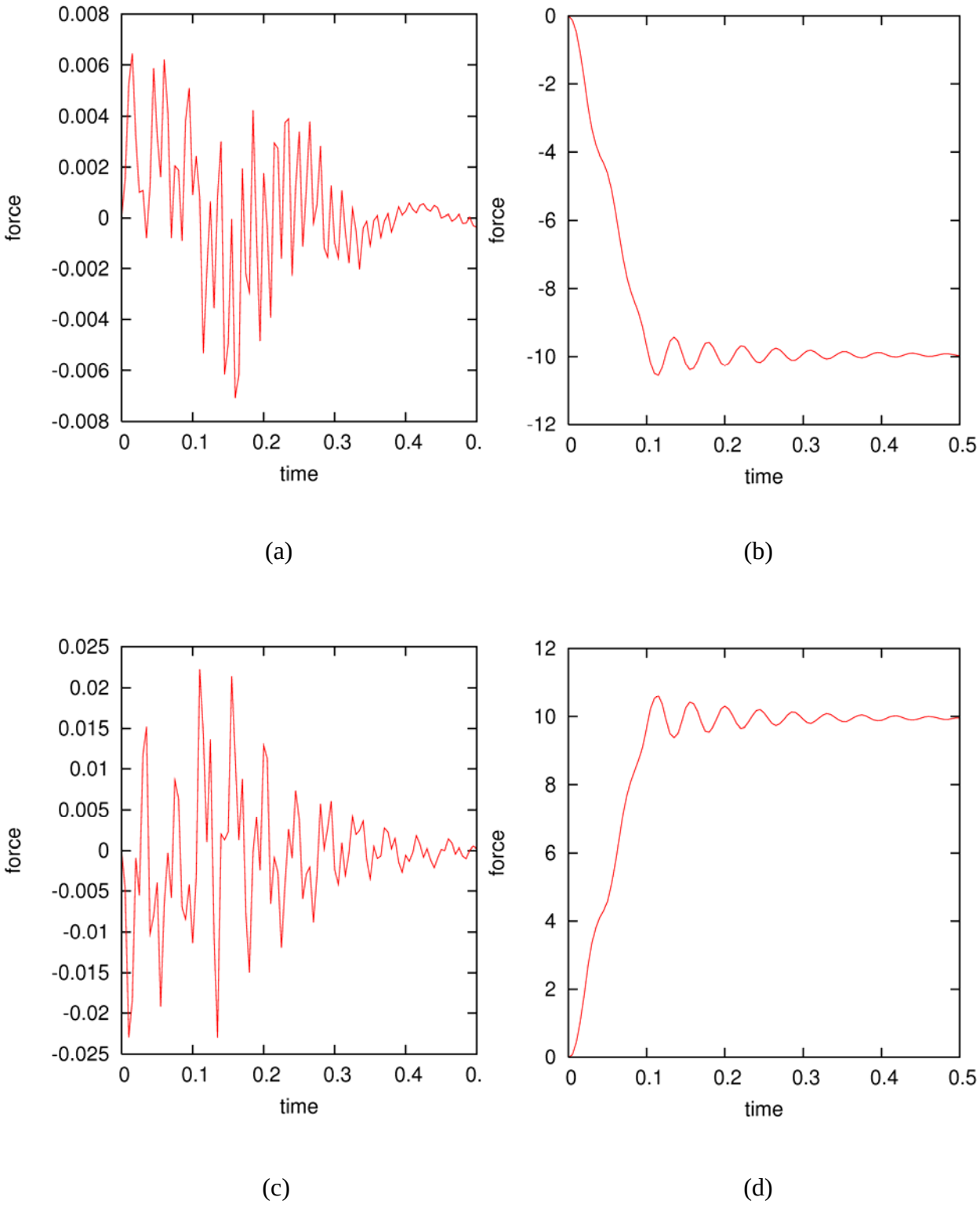

Figure 26. The total interface forces, F_x (a) and F_y (b), and the reaction forces, R_x (c) and R_y (d), developed for the shell edge tied to a shell surface (Type 7) interface. The expected peak forces are $F_x = R_x = 0.0$, $F_y = -10.0$, and $R_y = 10.0$.

6.7 TYPE 8: NODES SPOTWELDED TO A SURFACE

The nodes spotwelded to a surface algorithm is a penalty formulation that holds the "welded" slave nodes in place on the master surface until the failure criterion is satisfied. Once failure is detected, the surface behaves in the same manner as the Type 5 interface (discrete nodes on a surface). The failure criterion is expressed by:

$$\left(\frac{F_n}{F_{nf}}\right)^m + \left(\frac{F_s}{F_{sf}}\right)^n \geq 1$$

Where F_n and F_s are the current normal and shear forces, F_{nf} and F_{sf} are the specified normal and shear failure forces, and m and n are specified failure criterion exponents. Based on the penalty enforcement results for the Type 3 interface, a penalty stiffness factor of 10.0 is used for the analyses to prevent interpenetrations. The interface is evaluated for tensile failure and node-on-solid and node-on-shell interactions.

The tensile load is generated using a magnitude of P_y = -10.0 and is applied according to the time history in Figure 3 (a). The normal failure force, F_{nf} = 1.0, is determined from a desired failure load of 9.0, an assumed uniform stress distribution, the tributary area associated with each slave node, and failure criterion exponents m = n = 2. This approach averages the force distribution (due to tributary area) to determine an average nodal failure load for F_{nf}. As a result, the failure load for nodes along the interface edge is over predicted, while the failure load for nodes in the interface interior is under predicted. The shear failure force is set to a large value, F_{sf} = 10,000.0, in order for the normal force to dominate the failure criterion. Given the load time history, the applied body force will reach the expected failure load at time t = 0.09.

6.7.1 Type 8 Results

Prior to failure, relative normal displacements are controlled reasonably well (Figure 27). The peak relative normal displacements prior to failure are approximately 1.5E-03 for the node-on-solid scenario and 7.0E-03 for the node-on-shell scenario. The observed peak interface forces and failure times (Figure 28) are within a small margin of the expected failure load and failure

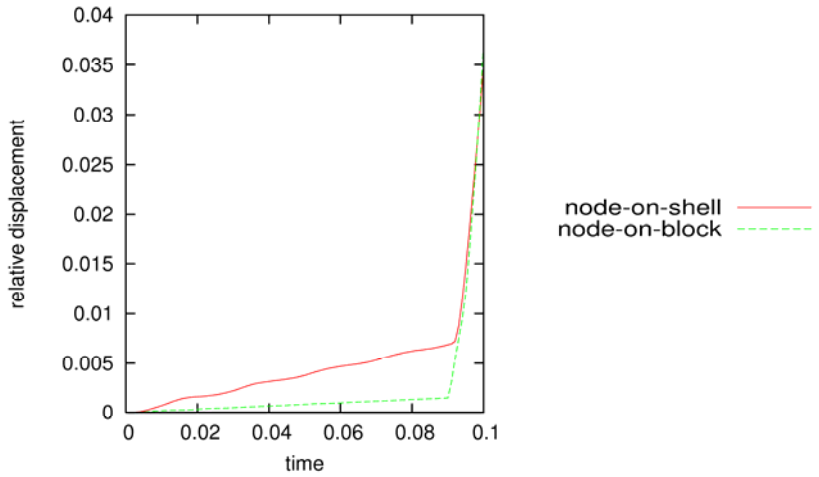

Figure 27. The relative y-displacements are reasonably small prior to failure (t ≈ 0.9) for the nodes spotwelded to a surface (Type 8) interface.

time. The node-on-shell scenario reaches a peak interface force of 9.08 at t = 0.091, and the node-on-solid scenario peaks at 8.94 at t = 0.089. The interface forces do not immediately fall to zero since the interface failure is progressive. Failure begins with the interior nodes, where the failure load is under predicted by the averaging process, and extends outward towards the edges, where the failure load is over predicted by the averaging process.

The chosen approach worked extremely well for the test problem. However, it is important to recognize that the interface parameters may need to be calibrated to produce the desired macro force response. This particular problem showed only minor sensitivity to the penalty stiffness factor. A penalty stiffness factor of 2.0 produced peak interface forces of 9.16 and 8.98, while a penalty stiffness factor of 20.0 produced peak interface forces of 9.05 and 8.96. The mesh discretization produced larger variations in the numerical results. Doubling the number of nodes in each coordinate direction reduced the peak interface forces to 8.66 and 8.56. This suggests that the interface parameters may need to be selected to fit a particular geometry and discretization.

6.7.2 Type 8 Summary

The spotwelded nodes algorithm captures the interface failure very well. The relative normal displacements prior to failure are larger than for other penalty enforcement algorithms with the same penalty stiffness factor, but the values are still reasonable. The interface parameters may need to be calibrated to produce the desired macro force response for a particular geometry and discretization.

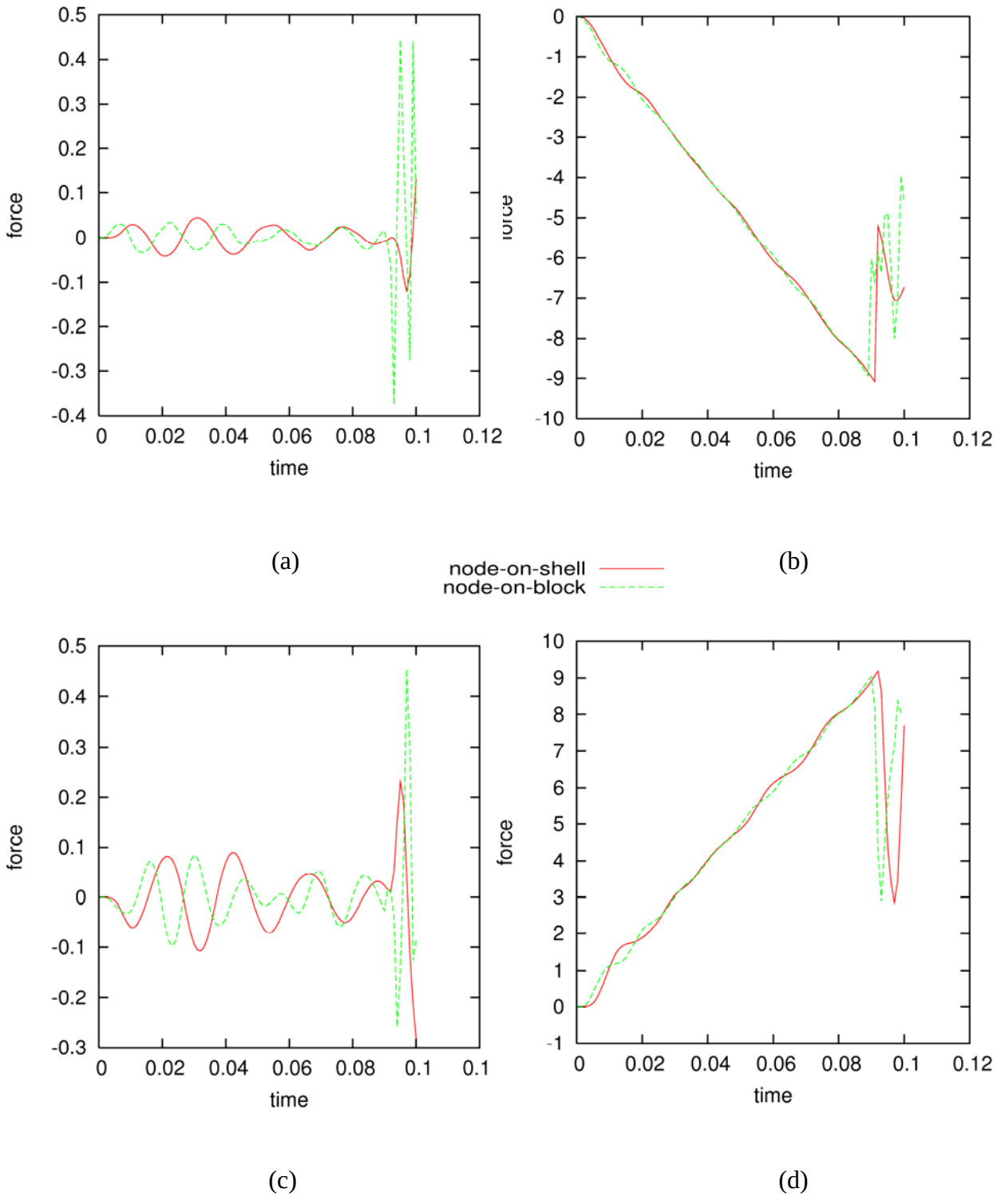

Figure 28. The interface forces, F_x (a) and F_y (b), and the reaction forces, R_x (c) and R_y (d) for the nodes spotwelded to a surface (Type 8) interface show that the interface failure occurs very close to the expected time (t = 0.09) and force (F_y = -9.0).

6.8 TYPE 9: TIED WITH FAILURE

The tied with failure contact algorithm is a penalty formulation that prevents relative movement of the slave and master surfaces in all coordinate directions until the failure criterion is satisfied. Once failure is detected, the surface behaves in the same manner as the Type 3 interface (sliding with separation and friction). The interface is restricted to continuum elements, so the only interaction considered is solid-on-solid. The interface segment failure criterion is expressed by:

$$\left(\frac{F_n}{F_{nf}}\right)^2 + \left(\frac{F_s}{F_{sf}}\right)^2 \geq 1$$

Where F_n and F_s are the current normal and shear forces, and F_{nf} and F_{sf} are the normal and shear failure forces. The normal and shear failure forces are calculated by the algorithm based upon the segment area and the specified normal and shear failure stresses. Two load cases are considered to examine the interface behavior during failure in pure tension and pure shear.

6.8.1 Type 9 with Tensile Failure

A pure tension load is applied to the upper block to examine whether the algorithm allows the slave and master surfaces to separate once the failure criterion is met. The tensile load is generated using a magnitude of P_y = -10.0 and is applied according to the time history in Figure 3 (a). The specified normal failure stress is σ_{nf} = 9.0, and the specified shear failure stress is a large value, σ_{sf} = 10,000.0, in order for the normal force to dominate the failure criterion. Since the slave surface has a total surface area of one square unit, the expected tensile failure load is 9.0. Given the load time history, the applied body force will reach the expected failure load at time t = 0.09, at which time the upper block should separate from the lower block.

Using the same penalty stiffness factor of 10.0 that was used for previous penalty enforcement analyses resulted in a peak normal interface force of 7.24, which is only 80% of the expected failure load. The initial failure occurs at a corner node on the upper block's right side, propagates along the right edge, and then progresses toward the body's left side. The normal stress components in the y-direction also reflect a non-homogeneous stress state in the elements closest to the interface. In the lower layer of the upper block, the y-stress component for the corner elements is 33% higher than for the center element. Due to the non-uniform stress state, the corner nodes satisfy the failure criterion at a much earlier macro load level than is analytically anticipated and initiate the progressive failure mode described earlier.

The non-uniform stress state results from the penalty enforcement algorithm. Consider the expected nodal loads for a uniform mesh and a uniform stress distribution. Accounting for tributary area, a corner node carries one-quarter the load of an interior node, while an edge node carries one-half the load of an interior node. For a homogeneous material, element stiffness contributions follow a similar pattern, and the resulting nodal displacements are uniform. When the penalty enforcement algorithm calculates the restoration force for a slave node, it is based upon the master segment stiffness, which is constant over the segment area. Therefore, restoration force variations, like those described above for a uniform stress distribution, produce a non-uniform gap between the master and slave surfaces. The resulting displacement field along the interface is consequently non-uniform, which produces a non-uniform stress state. As the penalty stiffness increases, the interface gap required to produce the restoration force is reduced,

and the resulting perturbations to the displacement and stress fields are lessened. Comparing the nodal restoration forces in the test problem to the expected forces from a uniform stress distribution shows that the restoration forces are 21% too high at the corner nodes, 11% too high at the edge nodes, and 12% too low at the interior nodes for a penalty stiffness factor of 10.0. Increasing the penalty stiffness factor to 100.0 reduced the force discrepancies. The restoration forces are up to 4% low at the corner nodes, 7% high at the edge nodes, and 1.5% high at the interior nodes. However, the penalty stiffness cannot be arbitrarily large, since very large penalty stiffness values can create numerical instabilities in the analysis.

The hourglass stabilization mode was also found to influence the predicted tensile failure load. For a penalty stiffness factor of 10.0, switching the hourglass stabilization mode from physical stabilization to a viscous form increased the peak interface force from 7.24 to 8.05. These results indicate that the interface and model parameters may need to be calibrated to produce the expected macro interface force behavior.

For the validation test problem, physical hourglass stabilization (Type 10) and a penalty stiffness factor of 100.0 were selected. The interface force time history (Figure 29 (a) and (b)) indicates that failure occurs at t = 0.085. The peak interface force in the y-direction is 8.43, which is 94% of the expected failure load. The interface failure is sudden, unlike the progressive failure seen for a penalty stiffness factor of 10.0. The stress distribution in the lower layer of the upper block is relatively uniform with a maximum variation in the y-stress component of 8%. The interface failure induces some dynamic oscillations in the reaction forces (Figure 29 (c) and (d)); otherwise, the reaction forces correspond very well to the interface forces. Overall, the interface behavior closely matches expectations.

6.8.2 Type 9 with Shear Failure

Compression is applied first to establish a normal force and check for interpenetration. The body force in the x-direction is then applied to generate a shear force. The body force magnitudes are $P_x = 4.0$ and $P_y = 10.0$, and the loads are applied according to the time history shown in Figure 3. The normal failure stress is specified as a large value, $\sigma_{nf} = 10{,}000.0$, in order for the shear force to dominate the failure criterion. The shear failure stress is specified as $\sigma_{sf} = 3.5$. Since the slave surface has a total surface area of one square unit, the expected shear failure load is 3.5, which is larger than the maximum static friction force of 3.0. Given the load time history, the body force in the x-direction will reach the failure load at time t = 0.3875, at which time the upper block should begin to slide along the lower block. When sliding occurs, F_x should correspond to the kinetic friction force of $f_k = 2.5$. A penalty stiffness factor of 10.0 is used for this test case.

The interface time history for F_x (Figure 30 (a)) shows the force build-up while the interface is tied, the peak interface force, and the post-failure frictional behavior. The shear failure occurs uniformly across the interface around t = 0.38. The peak value of F_x is 3.36, which is 96% of the expected shear failure force. The frictional behavior corresponds very well to the expected results with a rapid transition from the failure force to f_k. The interface failure induces some dynamic oscillations in R_x, but overall the reaction forces (Figure 30 (c) and (d)) agree very well with the interface forces.

6.8.3 Type 9 Summary

The "experimental" tied with failure contact algorithm enables two surfaces to be initially tied together and then be released when a failure criterion is satisfied. For the tension scenario, the interface demonstrated a rather high sensitivity to a variety of model parameters. Once the interface parameters were calibrated for the test problem, the tensile failure was captured quite well. The shear failure occurred very close to the expected failure load using the initially chosen model parameters. The interface's post-failure behavior corresponded very well with expectations.

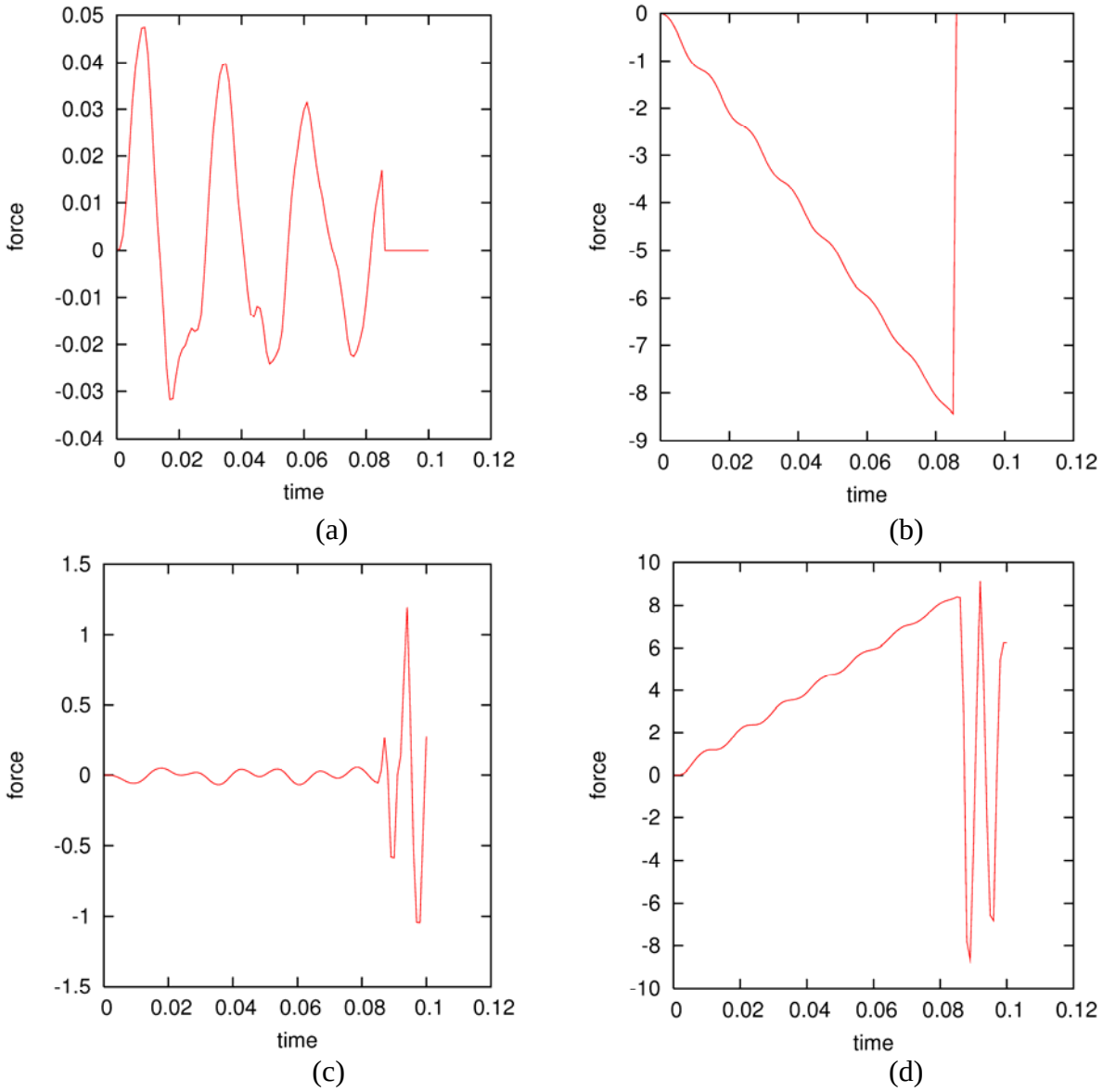

Figure 29. During tensile loading of the Type 9 interface, the interface forces, F_x (a) and F_y (b), indicate failure occurs a little earlier than the expected failure load F_y = -9.0. The reaction forces R_x (c) and R_y (d) exhibit some dynamic oscillations as a result of the interface failure.

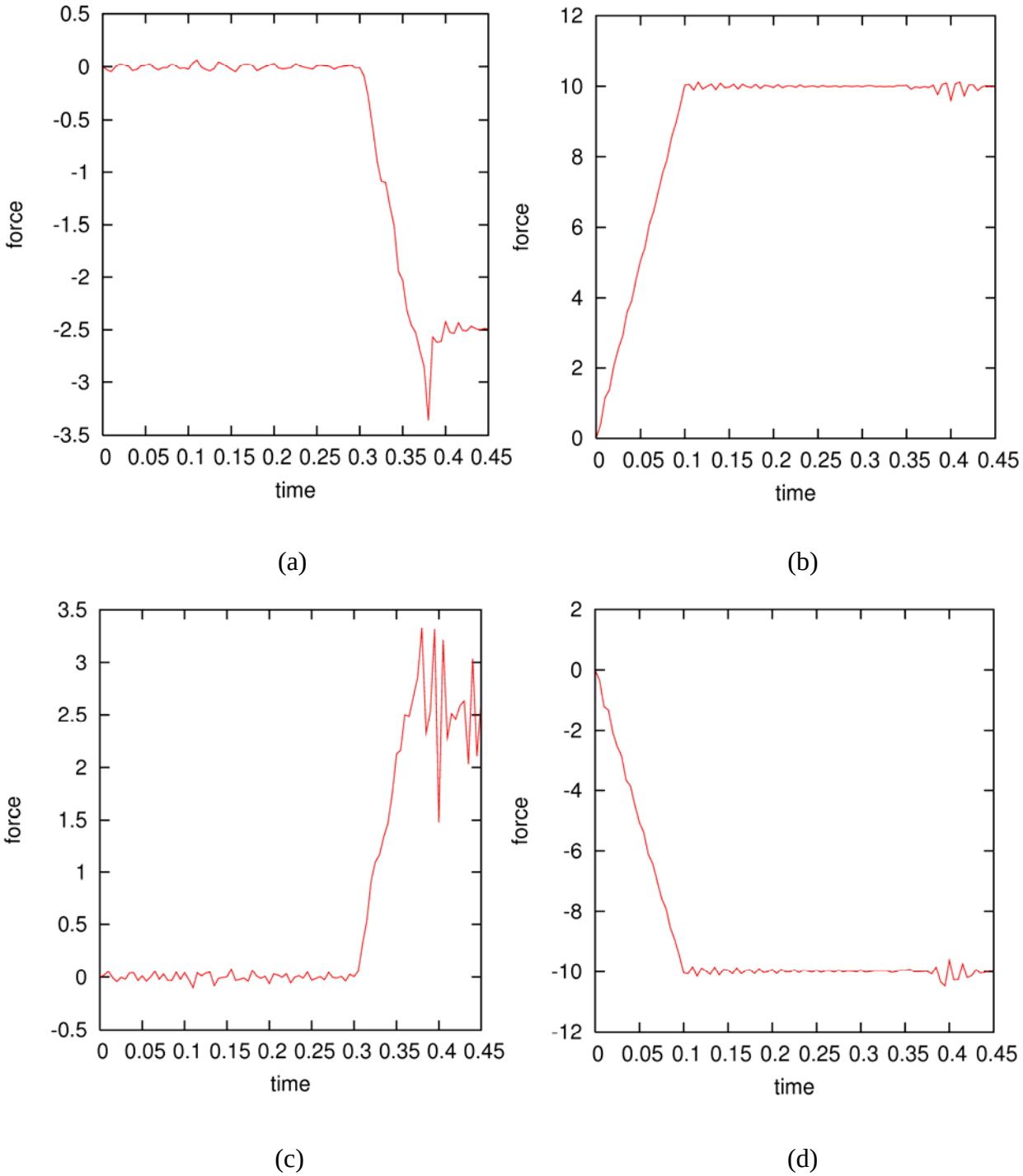

Figure 30. The interface force F_x (a) indicates that the Type 9 interface fails close to the expected shear failure load of 3.5. The interface force F_y (b) develops in response to the applied compressive loading (expected peak F_y = 10.0). The reaction forces R_x (c) and R_y (d) exhibit some dynamic oscillations resulting from the interface failure.

6.9 TYPE 10: ONE-WAY ALGORITHM FOR SLIDING WITH FRICTION OR SLIDING WITH SEPARATION AND FRICTION

The Type 10 algorithm is a single-pass formulation that provides two options for the interface behavior: sliding with friction or sliding with separation and friction. Contact is enforced by a penalty method for the sliding only option and by either a penalty or Lagrange method for the separation with friction option. The sliding with friction option provides an alternative penalty formulation to the kinematic algorithm used for the Type 1 interface; while the sliding with separation and friction option is a single pass alternative to the dual pass Type 3 interface. Since the algorithm is single pass, it is primarily intended for use when the master surface is much stiffer than the slave surface, e.g., when the master surface is part of a rigid body. Based upon the penalty enforcement results for the Type 3 interface, a penalty stiffness factor of 10.0 is used for the penalty enforcement option. The contact algorithm and enforcement options are evaluated for three types of element interaction: solid-on-solid, shell-on-solid, and shell-on-shell.

The problem geometry, applied loads, and expected results are virtually the same for all analyses. The initial shell-on-shell scenario exhibited large, high frequency oscillations for Lagrange contact enforcement and deformable bodies on the master and slave surfaces. To correct this problem, the shell elements forming the master surface were assigned to a rigid material for the shell-on-shell scenario and Lagrange enforcement option. This modification brings the problem definition more in line with the intended application of the interface.

Like the Type 3 interface, the contact algorithm is able to account for the shell element thickness. The body force magnitudes are $P_x = 3.1$ and $P_y = 10.0$, and the loads are applied according to the time history shown in Figure 3. The nodal time histories are generated using the nodal pairs given in Table 5 (a). The expected results are discussed in section 5.2.

6.9.1 Type 10 with Sliding Only

The mesh deformations exhibit the expected behavior. Relative normal displacements are prevented fairly well. The maximum interpenetration observed (Figure 31 (a)) is approximately 8.0E-03, which is similar to the Type 3 interface (refer to Figure 13 (b)). The total interface forces (Figure 32 (a) and (b)) show very good agreement with the expected normal and frictional forces. The peak observed friction force is 2.96 for solid-on-solid, 2.90 for shell-on-solid, and 2.88 for shell-on-shell. There is a quick transition from static to dynamic friction and the kinetic friction force is matched very well. The reaction forces (Figure 32 (c) and (d)) show a little more dynamic oscillation than the interface forces, but they still correspond very well to the expected time histories. The slave and master forces are balanced in all three coordinate directions.

6.9.2 Type 10 with Separation and Friction

For both enforcement options, the deformed states correspond very closely to the expected displacements. The slave and master surfaces are in balance throughout the analysis for penalty enforcement. The maximum interpenetration observed for the Lagrange method (Figure 31 (b)) is approximately 3.0E-04, which is an order of magnitude less than those for the penalty method (Figure 31 (a)). The relative normal displacements for both penalty methods (sliding only and sliding with separation and friction) were essentially identical.

For the most part, the total interface forces agree very well with the expected normal and frictional forces for both enforcement options. The penalty enforcement option results in peak friction forces of 2.96, 2.89, and 2.88 for the solid-on-solid, shell-on-solid, and shell-on-shell scenarios, respectively (Figure 33 (a) and (b)). The Lagrange enforcement option results in slightly lower peak friction forces of 2.89, 2.88, and 2.73 for the solid-on-solid, shell-on-solid, and shell-on-shell scenarios, respectively (Figure 34 (a) and (b)). The transition from static to dynamic friction is less rounded for the penalty method than the Lagrange method, but both methods provide a good representation of the expected response. The reaction forces (Figure 33 (c) and (d) and Figure 34 (c) and (d)) exhibit some oscillation, but they correspond very well to the expected time histories.

6.9.3 Type 10 Summary

The Type 10 interface behaves in a very similar manner to the Type 3 interface and did a good job capturing the expected response. The sliding only option represented the frictional behavior of the interface very well. Both the penalty and Lagrange enforcement options performed very well for the sliding with separation option. Like the Type 3 interface, the penalty option can be sensitive to the penalty stiffness factor, which may need to be adjusted for some problems.

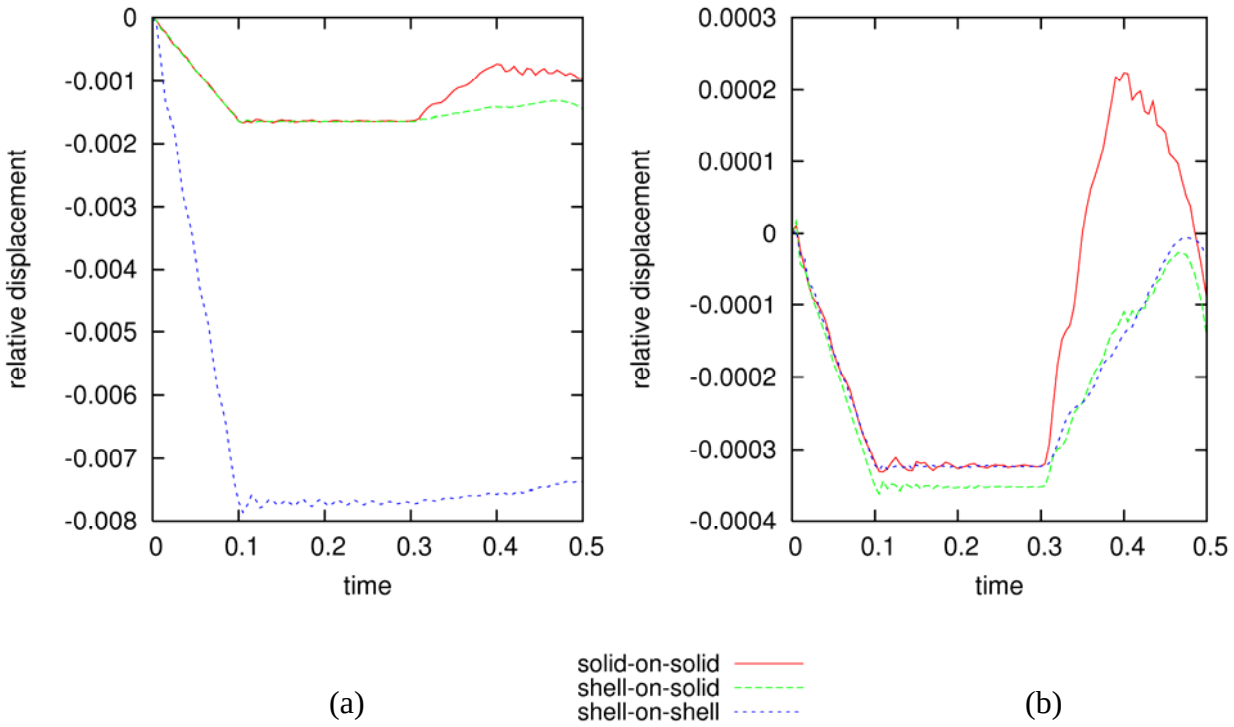

Figure 31. The relative y-displacements along the Type 10 interface for the penalty enforcement method (a) are an order of magnitude larger than those for the Lagrange enforcement option (b).

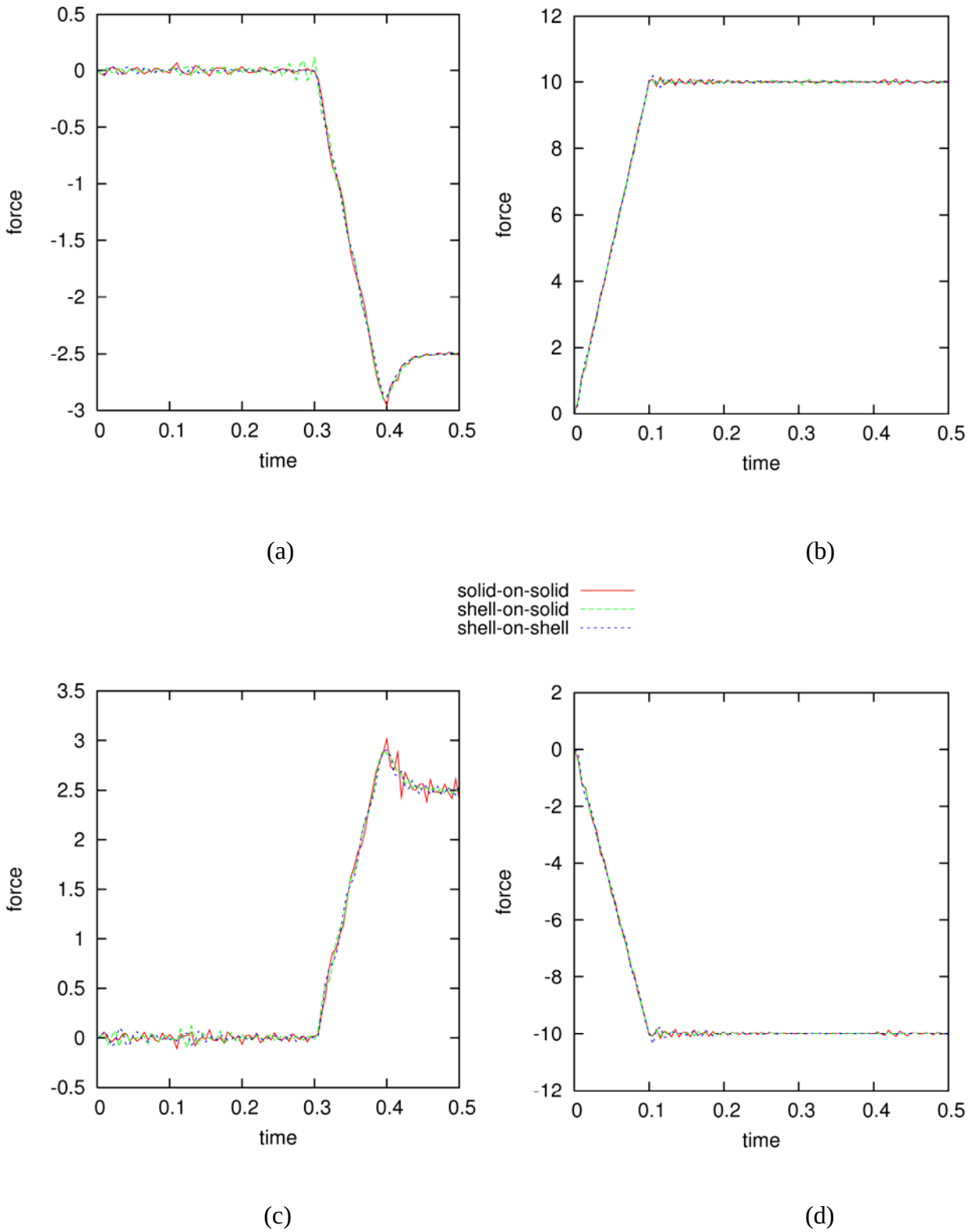

Figure 32. The interface forces F_x (a) and F_y (b) and the reaction forces R_x (c) and R_y (d) for the Type 10 interface with sliding only option. The expected friction forces are f_s = 3.0 and f_k = 2.5, and the expected peak normal forces are F_y = 10.0 and R_y = -10.0.

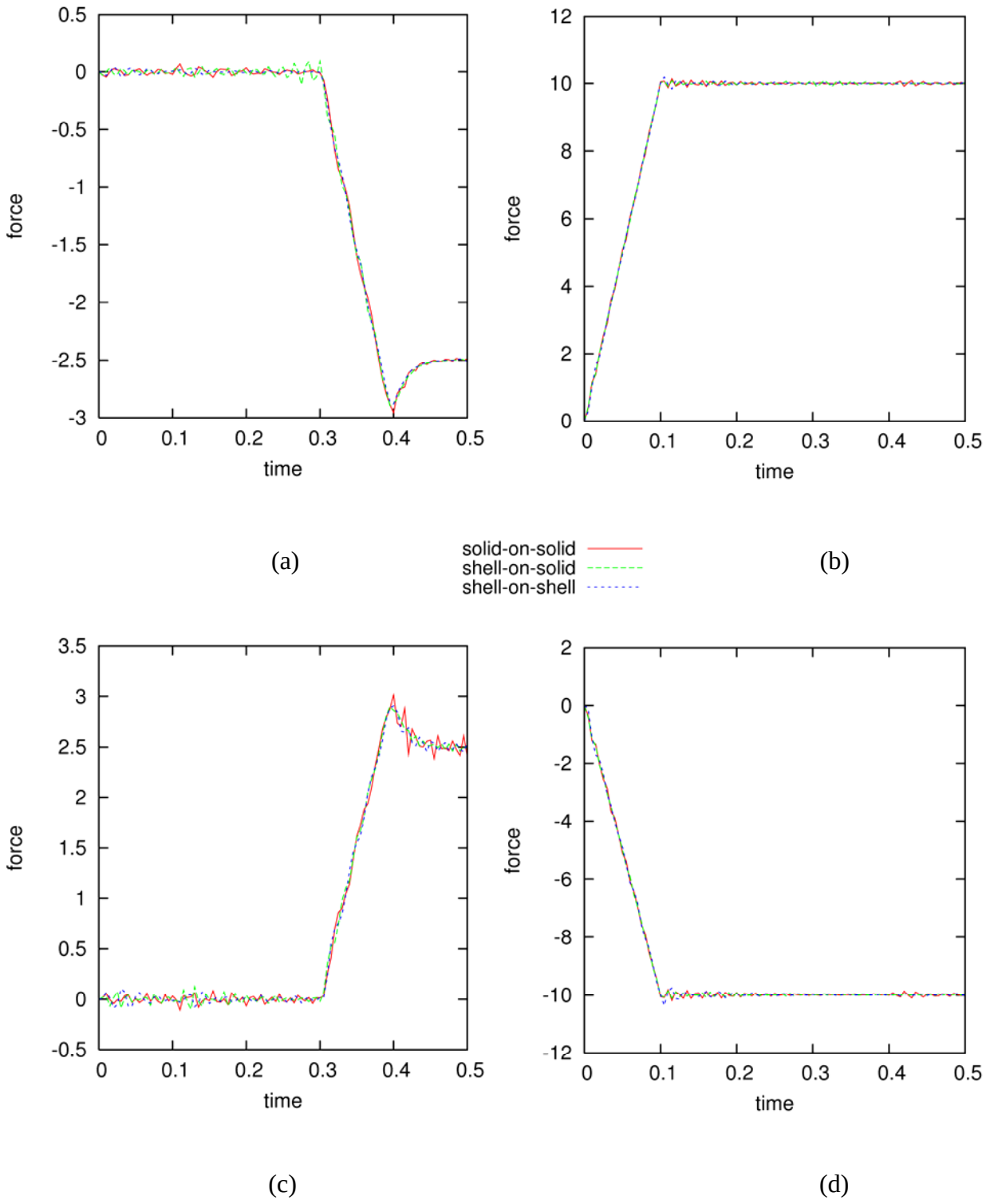

Figure 33. The interface forces, F_x (a) and F_y (b), and the reaction forces, R_x (c) and R_y (d), developed for the Type 10 interface's sliding with voids option with penalty enforcement. The expected friction forces are f_s = 3.0 and f_k = 2.5, and the expected peak normal forces are F_y = 10.0 and R_y = -10.0.

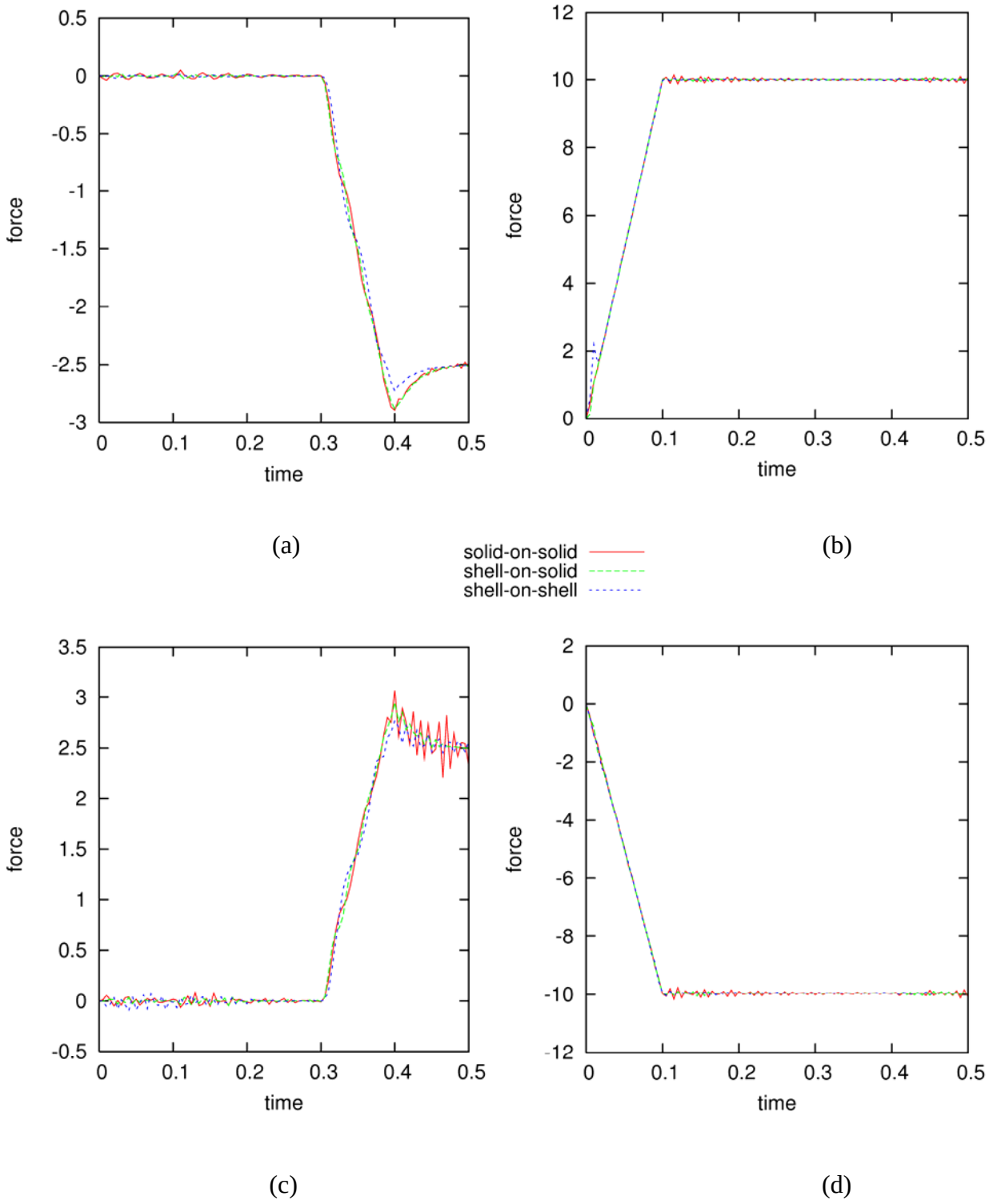

Figure 34. The interface forces, F_x (a) and F_y (b), and the reaction forces, R_x (c) and R_y (d), developed for the Type 10 interface's sliding with voids option with Lagrange enforcement. The expected friction forces are $f_s = 3.0$ and $f_k = 2.5$, and the expected peak normal forces are $F_y = 10.0$ and $R_y = -10.0$.

6.10 TYPE 12: AUTOMATIC CONTACT

The automatic contact algorithm uses a different search and detection methodology than the other contact algorithms in DYNA3D. It is a pseudo-dual pass formulation that automatically detects interfaces between bodies, treats all interface nodes as slave nodes, and treats all interface segments as belonging to the master surface. The underlying algorithms for interface Types 12, 13, and 14 are the same. The automatic contact behavior therefore needs to be examined only once. Contact can be enforced by either a penalty or Lagrange method. Based upon the penalty enforcement results for the Type 3 interface, a penalty stiffness factor of 10.0 is used for the penalty enforcement option. The contact algorithm and enforcement options are evaluated for three types of element interaction: solid-on-solid, shell-on-solid, and shell-on-shell.

Since the automatic contact algorithm uses internal vector blocks for data storage, an additional test case was run which extends the body in the z-direction. If the body shown in Figure 1 is considered a unit cell, then stacking additional unit cells in the z-direction creates a test case in which the applied loads and expected forces scale proportionally with the number of unit cells in the body. A body consisting of seventeen unit cells was used to ensure that more than sixty-five interface segments are on the contact surface.

The problem geometry, applied loads, and expected results are the same for all of the analyses. The contact algorithm accounts for the shell element thickness by default. The body force magnitudes are $P_x = 3.1$ and $P_y = 10.0$, and the loads are applied according to the time history shown in Figure 3. The domain limiting feature is utilized to minimize the computational effort required to identify the interface segments. Since all interface nodes are treated as slave nodes, the interface forces output by DYNA3D are not meaningful for automatic contact (refer to section 4.3). Therefore, the reaction forces are relied upon as an indirect measure of the interface forces. The global time step scale factor was reduced to 0.6 to help reduce the dynamic oscillations in the reaction force output. The nodal time histories are generated using the nodal pairs given in Table 5 (a). The expected results are discussed in section 5.2. For the extended body, the expected interface and reaction forces are a factor of seventeen greater than those developed for the basic contact problem. Consequently, the expected peak magnitude of F_y and R_y is 170.0, the expected peak friction force is 51.0, and the expected kinetic friction force is 42.5.

6.10.1 Type 12 with Penalty Enforcement

The mesh deformations correspond to expectations, and the relative normal displacements are prevented fairly well. The maximum interpenetration observed (Figure 35 (a)) is approximately 7.0E-03, which is very similar to the Type 3 interface penalty formulation (refer to Figure 13 (b)). The interface forces are on the order of 1E-15, so the forces on the upper and lower blocks are balanced. The reaction forces (Figure 36) exhibit some dynamic oscillation for both the single unit cell and the extended body, but the magnitudes and time histories correspond very well to the expected time histories. The peak friction forces observed in the single unit cell case are 3.02, 2.89, and 2.81 respectively for the solid-on-solid, shell-on-solid, and shell-on-shell scenarios. For the extended body, the peak friction forces observed are 51.3, 49.9, and 49.4 for the solid-on-solid, shell-on-solid, and shell-on-shell scenarios, respectively. The kinetic friction force is reflected very well in both cases.

6.10.2 Type 12 with Lagrange Enforcement

The mesh displacements reflect the expected deformations. The Lagrange enforcement method results in only a small amount of interpenetration. The maximum observed interpenetration (Figure 35 (b)) is approximately 2.5E-04, which is an order of magnitude less than the penalty method. The reaction forces (Figure 37) show some dynamic oscillation for both the single unit cell and the extended body. The peak friction forces observed in the single unit cell case are 2.95, 2.89, and 2.80 respectively for the solid-on-solid, shell-on-solid, and shell-on-shell scenarios. For the extended body, the peak friction forces observed are 50.5, 49.3, and 47.9 for the solid-on-solid, shell-on-solid, and shell-on-shell scenarios, respectively. Both cases reflect the kinetic friction force very well.

6.10.3 Type 12 Summary

Overall, the automatic contact algorithm performs very well. Since all interface nodes are treated as slave nodes, the total interface force acting on each block cannot be assessed directly; however, the interface forces can be inferred from the reaction forces generated on the lower block. The reaction forces from both the penalty and Lagrange enforcement methods correspond very well to the expected results, for both the single unit cell and extended body test cases.

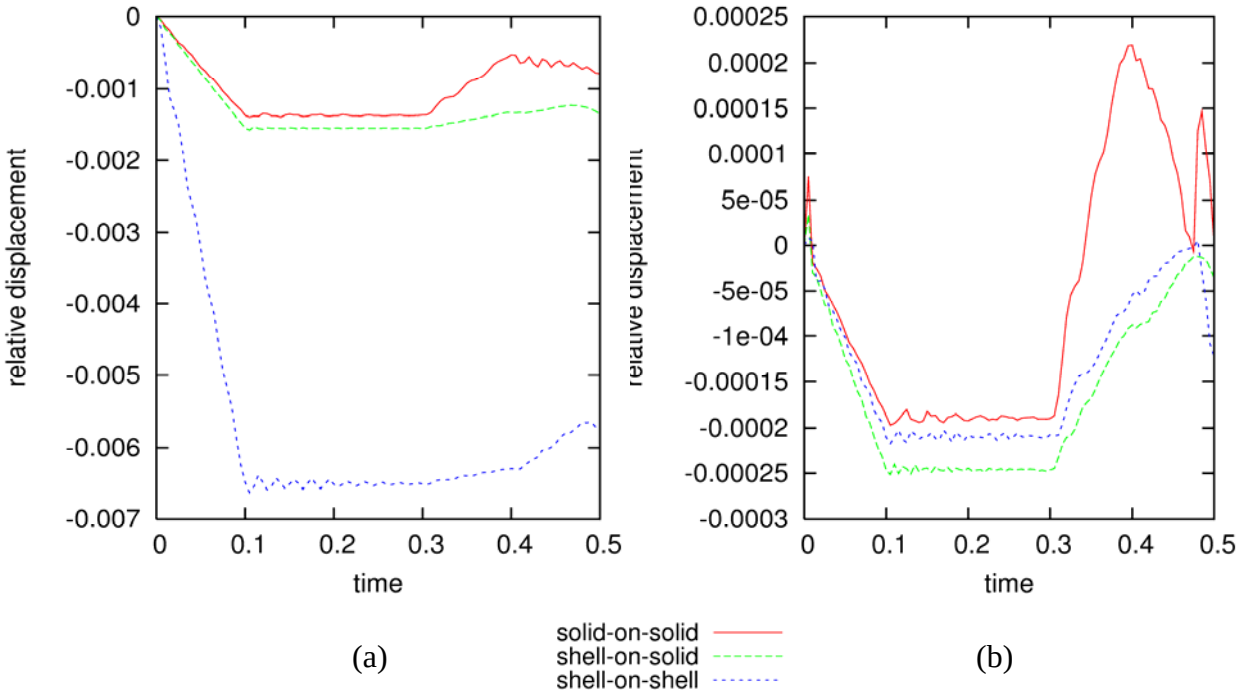

Figure 35. Although both Type 12 enforcement options prevent interpenetrations fairly well, the penalty method (a), with a penalty stiffness factor of 10.0, allows relative y-displacements that are an order of magnitude larger than those for the Lagrange method (b).

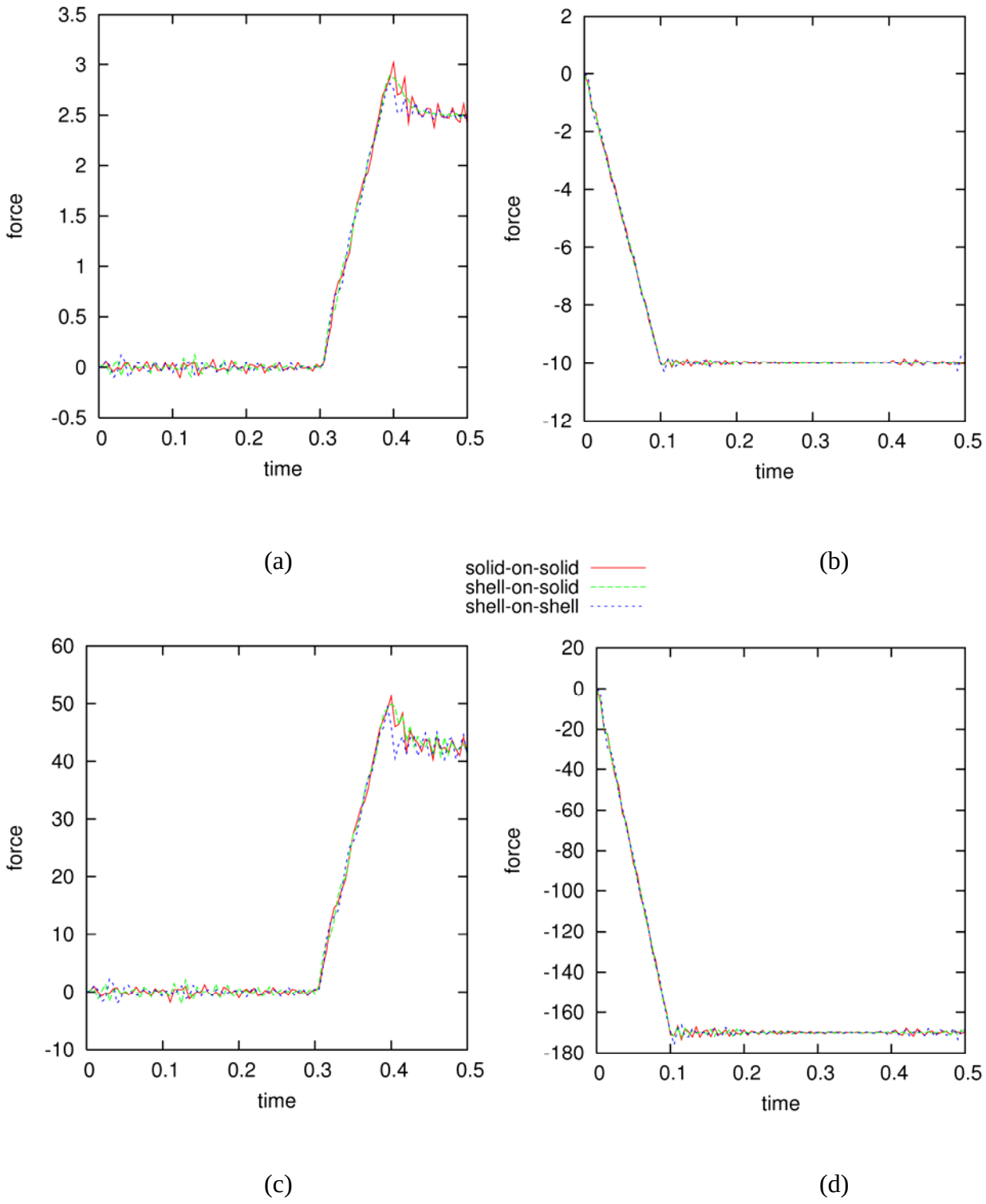

Figure 36. The single unit cell reaction forces R_x (a) and R_y (b) and the extended body reaction forces R_x (c) and R_y (d) developed by the Type 12 interface using the penalty enforcement option. The expected friction forces are $f_s = 3.0$ and $f_k = 2.5$ for the single unit cell and $f_s = 51.0$ and $f_k = 42.5$ for the extended body. The expected peak normal forces are $R_y = -10.0$ for the single unit cell and $R_y = -170.0$ for the extended body.

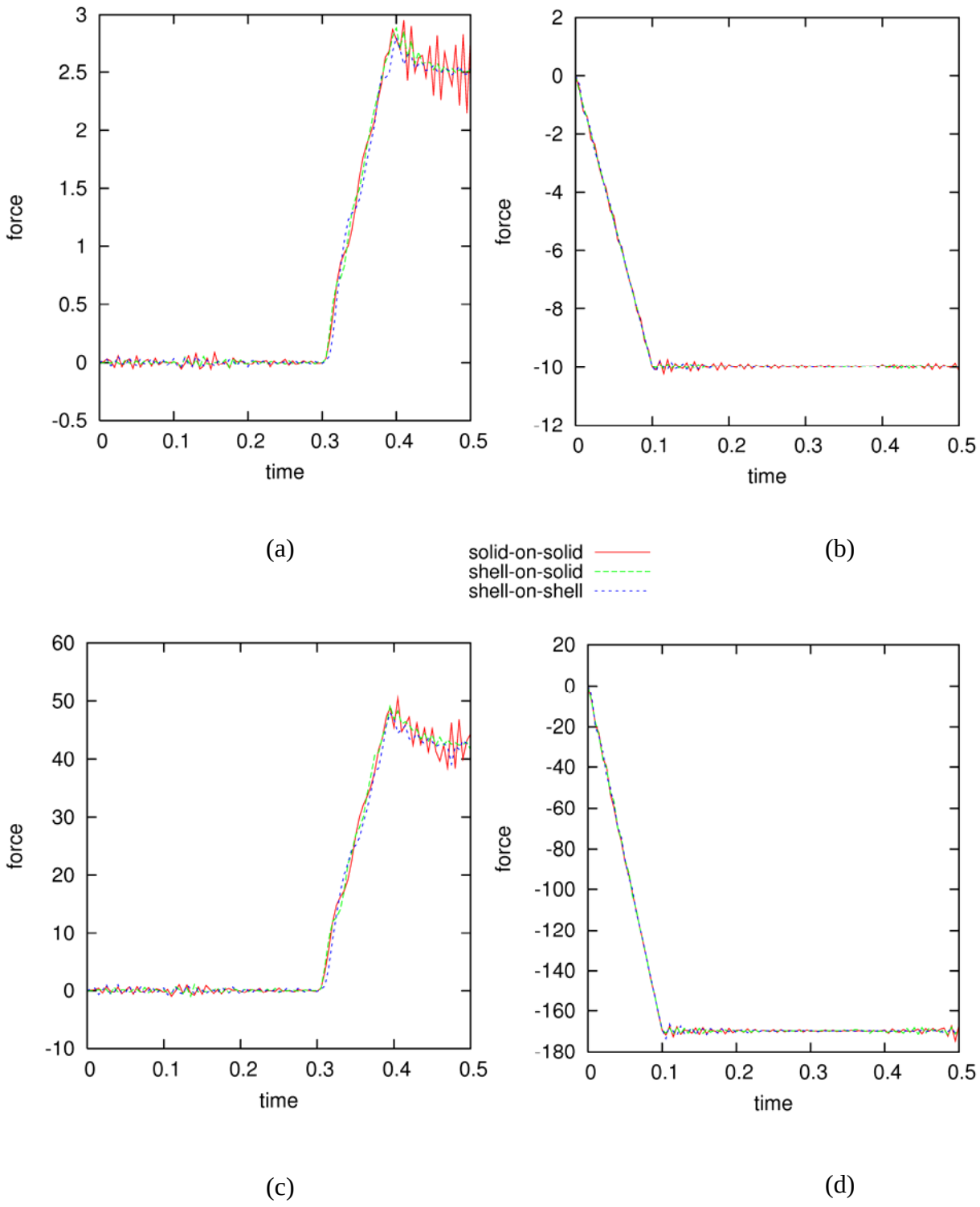

Figure 37. The single unit cell reaction forces R_x (a) and R_y (b) and the extended body reaction forces R_x (c) and R_y (d) developed by the Type 12 interface using the Lagrange enforcement option. The expected friction forces are $f_s = 3.0$ and $f_k = 2.5$ for the single unit cell and $f_s = 51.0$ and $f_k = 42.5$ for the extended body. The expected peak normal forces are $R_y = -10.0$ for the single unit cell and $R_y = -170.0$ for the extended body.

7 SUMMARY OF INTERFACE BEHAVIOR

The basic contact test suite demonstrates the versatility and capabilities of the DYNA3D contact algorithms to simulate tied, frictional, and frictionless interfaces for a variety of element types and element interactions. Interface behavior is evaluated with respect to observed deformations, nodal time histories, interface forces, and reaction forces. Overall, the contact algorithms do a very good job representing the interface behavior. Observed mesh deformations closely match expectations, and relative displacement plots confirm that interpenetrations are limited to reasonable amounts. Normal and tangential forces are resolved very well for the interfaces, and the reaction forces demonstrate that the interfaces transfer the appropriate forces between bodies.

The interfaces are able to enforce kinematic restrictions in both the normal and tangential directions. The kinematic and Lagrange enforcement methods tend to limit interpenetration more effectively than the penalty enforcement method, even with an increased penalty stiffness scale factor (which can adversely affect the analysis stability and time-step size). Nodal interpenetrations are on the order of 10^{-4} for the kinematic and Lagrange enforcement options and 10^{-3} for penalty enforcement. However, the penalty enforcement option tended to resolve the peak friction force and the transition from static to dynamic friction better than the Lagrange method. The peak friction force was resolved to within 95-99% of the theoretical peak by the penalty enforcement option, compared to within 91-96% for Lagrange enforcement. The exponential friction law in DYNA3D produces a more rounded transition from static to dynamic friction than the sharp, theoretical step-function. The dynamic effects included in the DYNA3D analysis also introduce some oscillations to the results.

The most significant variations from the expected results were observed for the Type 1 interface. The manner in which forces are distributed to master segments resulted in a force imbalance between the master and slave surfaces. Changes to the kinematic enforcement algorithm are being evaluated to correct the behavior. Additionally, the interface failure algorithms (Types 8 and 9) exhibited sensitivity to a variety of model parameters. Consequently, the interface failure models may need to be calibrated to obtain the correct macro failure load.

Multi-surface contact behavior is addressed in a companion report (McMichael, 2006).

REFERENCES

1. Lin, J. I., "DYNA3D: A Nonlinear, Explicit Three-Dimensional Finite Element Code for Solid and Structural Mechanics, User Manual," University of California Lawrence Livermore National Laboratory, UCRL-MA-107254, **2005**.
2. McMichael, L. D., "Contact Interface Verification for DYNA3D, Scenario 2: Multi-Surface Contact," University of California Lawrence Livermore National Laboratory, UCRL-TR-221292, **2006**.

APPENDIX A: TEST PROBLEMS

File Name	Problem Description
sslide1k.dyn	Type 1 interface with kinematic enforcement.
sslide2kc.dyn	Type 2 interface with kinematic enforcement and compression loading.
sslide2kt.dyn	Type 2 interface with kinematic enforcement and tension loading.
sslide3l.dyn	Type 3 interface with Lagrange enforcement.
sslide3p.dyn	Type 3 interface with penalty enforcement.
sslide5l.dyn	Type 5 interface with Lagrange enforcement.
sslide5p.dyn	Type 5 interface with penalty enforcement.
sslide6k.dyn	Type 6 interface with kinematic enforcement.
sslide7k.dyn	Type 7 interface with kinematic enforcement.
sslide8p.dyn	Type 8 interface with penalty enforcement.
sslide9ps.dyn	Type 9 interface with penalty enforcement and shear failure.
sslide9pt.dyn	Type 9 interface with penalty enforcement and tension failure.
sslide10lr.dyn	Type 10 interface with Lagrange enforcement.
sslide10psl.dyn	Type 10 interface with penalty enforcement and sliding only.
sslide10pv.dyn	Type 10 interface with penalty enforcement and sliding with voids.
sslide12l.dyn	Type 12 interface with Lagrange enforcement.
sslide12p.dyn	Type 12 interface with penalty enforcement.
sslide12l_vec.dyn	Type 12 interface with Lagrange enforcement and multiple unit cells.
sslide12p_vec.dyn	Type 12 interface with penalty enforcement and multiple unit cells.